



Comparative proteomic study of phytotoxic effects of silver nanoparticles and silver ions on tobacco plants

Petra Peharec Štefanić¹ · Martina Jarnević¹ · Petra Cvjetko¹ · Renata Biba¹ · Sandra Šikić² · Mirta Tkalec¹ · Mario Cindrić³ · Ilse Letofsky-Papst⁴ · Biljana Balen¹

Received: 3 January 2019 / Accepted: 22 May 2019
© Springer-Verlag GmbH Germany, part of Springer Nature 2019

Abstract

Widespread application of silver nanoparticles (AgNPs), due to their antibacterial and antifungal properties, increases their release into the environment and potential detrimental impact on living organisms. Plants may serve as a potential pathway for AgNPs bioaccumulation and a route into the food chain, hence investigation of AgNP phytotoxic effects are of particular importance. Since proteins are directly involved in stress response, studies of their abundance changes can help elucidate the mechanism of the AgNP-mediated phytotoxicity. In this study, we investigated proteomic changes in tobacco (*Nicotiana tabacum*) exposed to AgNPs and ionic silver (AgNO₃). A high overlap of differently abundant proteins was found in root after exposure to both treatments, while in leaf, almost a half of the proteins exhibited different abundance level between treatments, indicating tissue-specific responses. Majority of the identified proteins were down-regulated in both tissues after exposure to either AgNPs or AgNO₃; in roots, the most affected proteins were those involved in response to abiotic and biotic stimuli and oxidative stress, while in leaf, both treatments had the most prominent effect on photosynthesis-related proteins. However, since AgNPs induced higher suppression of protein abundance than AgNO₃, we conclude that AgNP effects can, at least partially, be attributed to nanoparticle form.

Keywords Silver nanoparticles · Silver nitrate · *Nicotiana tabacum* · Two-dimensional electrophoresis · Proteomics · Phytotoxicity

Responsible editor: Gangrong Shi

Electronic supplementary material The online version of this article (<https://doi.org/10.1007/s11356-019-05552-w>) contains supplementary material, which is available to authorized users.

✉ Biljana Balen
bbalen@biol.pmf.hr

¹ Department of Biology, Faculty of Science, University of Zagreb, Horvatovac 102a, HR-10000 Zagreb, Croatia

² Department of Ecology, Institute of Public Health “Dr. Andrija Štampar”, Mirogojska cesta 16, HR-10000 Zagreb, Croatia

³ Ruđer Bošković Institute, POB 1016, HR-10000 Zagreb, Croatia

⁴ Institute of Electron Microscopy and Nanoanalysis (FELMI), Graz University of Technology, Graz Centre for Electron Microscopy (ZFE), Austrian Cooperative Research (ACR), Steyrergasse 17, 8010 Graz, Austria

Introduction

Nanomaterials are chemical substances of which a single unit is sized on the nanoscale, namely, between 1 and 100 nm. They are developed to exhibit novel characteristics compared to the same material without nanoscale features, such as increased strength, chemical reactivity, or conductivity. Among different types of nanomaterials, one of the most frequently used ones are silver nanoparticles (AgNPs) owing to antibacterial and antifungal properties of silver; therefore, they are applied in the production of paints, cosmetics, textiles, and sports equipment (Zhang et al. 2016). Moreover, due to high electrical and thermal conductivity, AgNPs are increasingly being implemented in the numerous consumer products and agriculture (Zhang et al. 2016). Increased production will inevitably increase the potential for their release into the environment (McGillicuddy et al. 2017), which may result in contamination of soil and water resources. It has been reported that AgNPs released to the natural environment undergo

profound chemical transformations that can affect their stability and bioavailability, and thus increase their toxicity on living organisms, including bacteria, fungi, algae, plants, vertebrates, invertebrates, and human cells (Levard et al. 2012).

Plants play a significant role in accumulation and biodistribution of many environmentally released substances; therefore, they may serve as a potential pathway for AgNPs uptake, bioaccumulation, and a route into the food chain (Rico et al. 2011). Hence, the phytotoxic effects of AgNPs should be given a particular attention. Toxicological studies dealing with the effects of AgNPs on plants conducted so far indicate that plants can take up and accumulate AgNPs and translocate them in different plant organs, thus affecting growth and development processes (Cvjetko et al. 2017). Moreover, it was shown that plant exposure to AgNPs can result in increased oxidative damage of lipids, proteins, and DNA molecule as well as in changes in the activity of antioxidant enzymes (Cvjetko et al. 2017; Cvjetko et al. 2018; Peharec Štefanić et al. 2018), which suggests that oxidative stress has an important role in the phytotoxicity of AgNPs.

Previously, we have investigated the toxic effects of laboratory synthesized citrate-coated AgNPs on the tobacco (*Nicotiana tabacum* L.) adult plants and found that AgNPs were less toxic than the corresponding AgNO₃ treatments (Cvjetko et al. 2018). Namely, exposure to AgNPs induced significant oxidative stress neither in roots nor in leaves, although changes in activity of some antioxidant enzymes were recorded. Furthermore, microscopy observations revealed that the treatment with 100 μM AgNPs induced high vacuolization of root cells due to the direct uptake of nanoparticles, while in leaves, changes in chloroplast ultrastructure were detected. In this study, our aim was to examine the molecular basis of the observed AgNP phytotoxicity; therefore, we analyzed the proteomes of roots and leaves of adult plants exposed to treatments with 100 μM AgNPs. Proteomic techniques, which detect quantitative and qualitative changes in protein expression profiles, are powerful tools for the identification of proteins related to specific developmental and/or environmental signal (Rogić et al. 2015). Proteomics can provide new information to improve the knowledge of interactions between plants and nanoparticles, since these studies reflect the nanoparticle effects on gene expression. So far, proteomic-based approach for studying plant responses to AgNP-induced stress has been employed in only a few studies reporting that AgNPs can interact with different cell metabolic processes such as protein synthesis/degradation and apoptosis (Mirzajani et al. 2014), primary metabolism and cell defense (Vannini et al. 2014), stress and signalling (Mustafa et al. 2015), redox regulation, and the sulphur metabolism (Vannini et al. 2013). In the present study, AgNP-induced changes in the proteome profiles of roots and leaves of tobacco plants were evaluated and compared to the effects induced by treatments with ionic

silver (AgNO₃) in order to elucidate the mechanism of AgNP-mediated phytotoxicity.

Materials and methods

Exposure solutions

We used commercial citrate-coated AgNPs (50 nm Silver Nanospheres, Citrate, BioPureTM, Nanocomposix, San Diego CA, with ζ potential of − 47 mV). The concentration of AgNP stock solution was 1 mg cm^{−3}. AgNPs in stock solution were examined with monochromated TF20 (FEI Tecnai G2) transmission electron microscope (TEM).

For treatment of tobacco plants in this study, AgNP stock solution was dissolved in ultrapure ion-free Milli-Q® (Millipore, 18.2 MΩ-cm resistivity) water to obtain a 100 μM concentration (based on concentration of total Ag). Ag concentration in AgNP solution was further confirmed by ELAN DRC-e inductively coupled plasma mass spectrometry (ICP-MS) (Perkin Elmer, USA) as described in the “[AgNPs localization and Ag uptake determination](#)” section. For treatments with ionic silver, silver nitrate (AgNO₃, Sigma-Aldrich) was dissolved in ultrapure Milli-Q® water to obtain a 100 μM solution.

Stability evaluation of AgNPs

For AgNP stability estimation, an aliquot (1 cm³) of the 100 μM AgNP solution was pipetted to the 1-cm quartz cuvette for spectrophotometric absorbance measurements, which were performed using the UV-visible spectrophotometer (Specord 50 PLUS, Analytik Jena, Germany) in the wavelength range of 300–800 nm. For instrument zeroing, Milli-Q® water was used. AgNP stability was monitored during 7 days (treatment duration). Based on the results obtained by spectrophotometric measurements, the 2nd, the 5th, and the 7th day were chosen for further analyses of AgNP stability. Hydrodynamic diameter and charge of AgNPs in Milli-Q® water were measured using Zetasizer Nano ZS (Malvern, UK) equipped with green laser (532 nm). The data processing was done by the Zetasizer software 6.32 (Malvern instruments). Silver dissolution was determined by centrifugal ultrafiltration (Millipore Amicon Ultra-4 3K) through a membrane with a 3-kDa molecular weight limit. Suspensions were centrifuged for 40 min at 15000×g. The silver concentration in the filtrate was determined using ELAN DRC-e ICP-MS (Perkin Elmer, USA). Silver concentration was calculated according to the calibration curve obtained with a set of standards of known concentrations and related to the Ag concentration before ultrafiltration to calculate dissolved Ag⁺ ions.

Plant material and treatments

Propagation of *Nicotiana tabacum* L. cv Burley adult plants was conducted as previously described (Cvjetko et al. 2018). Two-month-old plants were placed in Milli-Q® water supplemented with either AgNPs or AgNO₃ applied in the 100 µM concentration and treated for 7 days. Control plants were kept in the Milli-Q® water, free of AgNPs or AgNO₃. After the treatment, roots and leaves were separated. Roots were washed with 0.01 M HNO₃ and subsequently rinsed with Milli-Q® water to remove the AgNPs attached to root tissue. All tissue samples were lyophilized.

AgNPs localization and Ag uptake determination

For localization of AgNPs in cells, small pieces of roots and leaves were prepared as previously described (Cvjetko et al. 2018; Peharec Štefanić et al. 2018) and were examined with monochromated TF20 (FEI Tecnai G2) TEM.

To determine total Ag concentration, measurements were performed by applying the same protocol as reported in Cvjetko et al. (2018) using the ELAN DRC-e ICP-MS (Perkin Elmer, USA). Silver concentration was calculated according to the calibration curve obtained with a set of standards of known concentrations. Detection limits and limit of quantification (LOQ) were 0.2 and 1 mg kg⁻¹, respectively. Spike recovery tests were 96.2 and 96.6% for roots of AgNP-treated and AgNO₃-treated plants, respectively, and 95.4 and 95.6% for leaves of AgNP-treated and AgNO₃-treated plants, respectively.

Protein extraction and quantification

For protein extraction, 0.15 g of lyophilized tissue was weighed and proteins were extracted in the 6 cm³ of extraction buffer (500 mM Tris, 50 mM ethylenediaminetetraacetic acid (EDTA), 700 mM sucrose, 100 mM potassium chloride (KCl), 1 mM phenylmethylsulfonyl fluoride (PMSF), and 2% β-mercaptoethanol) using precooled mortar and pestle. Three replicates for each tissue type of the control and each treatment were prepared. Homogenates were transferred in 15 cm³ Falcon tubes, stirred on vortex, and incubated horizontally on ice for 10 min. After incubation of homogenates, extraction with phenol was further applied according to the protocol of Pavoković et al. (2012). Proteins were precipitated overnight at -20 °C using the ice-cold precipitation solution (0.1 M ammonium acetate (NH₄CH₃CO₂) in methanol). Solutions with precipitated proteins were centrifuged at 3900×g for 15 min at +4 °C, after which pellet was washed 3× with 3 cm³ of ice-cold precipitation solution and 1× (last washing) with 3 cm³ ice-cold acetone. Between each washing step, samples were centrifuged at 3900×g for 15 min at +4 °C. Protein pellets were air-dried and dissolved in 500 mm³ of

isoelectric focusing (IEF) buffer (9 M urea and 4% (w/v) 3-((3-cholamidopropyl) dimethylammonio)-1-propanesulfonate (CHAPS)), which was supplemented with 2 mg cm⁻³ of dithiothreitol (DTT) and 5.2 mm³ of ampholytes. Dissolved pellets were transferred in 1.5 cm³ plastic tubes and centrifuged at 20,800×g for 5 min at room temperature, and obtained supernatants were used for determination of protein concentration according to the modified Bradford method (Pavoković et al. 2012) using bovine serum albumin (BSA) as a standard.

Two-dimensional electrophoresis (2-DE)

The sample volume, which contained 500 µg of proteins, was mixed with IEF buffer (containing DTT and ampholytes) to obtain the total volume of 400 mm³ (volume for loading on dry immobilized pH gradient (IPG) strips). Additionally, in each sample, 5 mm³ of bromophenol blue was added and samples were vortexed and centrifuged at 20,800×g for 5 min at room temperature. For the rehydration step, supernatants were transferred to the wells of the rehydration tray with IPG strips (Immobiline DryStrip, 13 cm, pH 3–10 NL, GE Healthcare, USA), which were covered with 900 mm³ of cover fluid (Immobiline DryStrip Cover Fluid, GE Healthcare, USA) and left for rehydration for 14 h at room temperature.

The separation of proteins by two-dimensional electrophoresis (2-DE) was performed as described in Rogić et al. (2015), with some modifications. After the rehydration, IPG strips were placed on the top of the manifold of the Ettan IPGphor 3 system (GE Healthcare, USA) for the 1st step of protein separation, using the following IEF programme: 500 V for 1 h (step and hold), 1000 V for 1 h (gradient), 8000 V for 3 h (gradient), and 8000 V for 4 h (step and hold), until a total run of 45,000 V h was achieved. After the IEF was finished, IPG strips were stored at -80 °C.

Prior to the 2nd step of protein separation, sodium dodecyl sulphate-polyacrylamide gel electrophoresis (SDS-PAGE), IPG strips were defrosted and incubated for 15 min in 2.5 cm³ of equilibration buffer (0.05 M Tris-HCl pH 8.8, 6 M urea, 2% SDS (w/v)) containing 130 mM DTT, and after that for 15 min in the buffer of the same composition, but with 135 mM iodoacetamide instead of DTT. Equilibrated gels were soaked in electrode buffer (0.025 M Tris, 0.192 M glycine, 10% (w/v) SDS, pH 8.3) and placed on the top of the vertical polyacrylamide slab gel (12% T, 2.67% C, with the addition of 10% SDS). SDS-PAGE was performed using the PROTEAN II xi system (BioRad, USA) and has been run first at 100 V for 30 min, and then at 220 V till the end (approximately 5 h).

Protein spots were visualized by Commassie Brilliant Blue (CBB) R-250 staining solution (0.1% (w/v) CBB, 45% (v/v) methanol, and 10% (v/v) glacial acetic acid), scanned for image acquisition and data analysis.

Image acquisition and data analysis

For analyses of root and leaf proteomes, the whole experiment was repeated 3×, with 3 technical replicates for each sample. 2-D gels were scanned with image scanner (Epson Perfection, V700 Photo, USA) at 600-dpi resolution. Acquired images were quantitatively and qualitatively analyzed using the ImageMaster 2D Platinum software version 7.0 (GE Healthcare, USA). The abundance of each spot on 2-D gels was estimated based on the volume percentage. Protein spots that exhibited ± 1.5 -fold change with statistical significance $P \leq 0.05$ (ANOVA, STATISTICA 13.3, TIBCO Software Inc.) were considered as differently abundant and analyzed with mass spectrometry. Subsequently, the dataset consisting of relative abundance values of proteins was analyzed by principal component analysis (PCA), for each tissue separately using STATISTICA 13.3, TIBCO Software Inc.

Protein digestion and peptide extraction and purification

Spots of differentially abundant proteins were excised from the gels with a pipette tip and destained in the solution composed of 10% (v/v) acetic acid and 20% (v/v) methanol, after which they were conditioned for trypsin digestion: firstly, in 50 mM ammonium bicarbonate (NH_4HCO_3), pH 7.8, then in the 50:50 (v/v) of 50 mM NH_4HCO_3 (pH 7.8)/acetonitrile solution, and finally, in 100% acetonitrile. After drying in vacuum centrifuge (Concentrator 5301, Eppendorf, Germany), gel pieces were submerged to trypsin digestion ($10 \mu\text{g cm}^{-3}$ trypsin solution in 25 mM NH_4HCO_3 , pH 7.8, using sequencing-grade trypsin (Roche, USA)) in thermomixer at 500 rpm and 37 °C for 18 h. After digestion, proteins were extracted from gel pieces with extraction solution (50% (v/v) of 5% trifluoroacetic acid (TFA) in acetonitrile) by incubation in ultrasonic bath (Ultrasonic Cell Disruptor XL, Misonix Inc., USA) at room temperature, after which they were dried in vacuum centrifuge and stored at -80 °C. Extracted peptides were dissolved in 35 mm³ of 0.1% (v/v) TFA, purified using the Bravo Automated Liquid Handling Platform on RP-S cartridges (AssayMAP Bravo, Agilent Technologies, USA), and dried.

Mass spectrometry analysis

For protein analyses, matrix-assisted laser desorption/ionization–time-of-flight mass spectrometry (MALDI) was applied. Purified and dried peptides were dissolved in 2 mm³ of 5 mg cm⁻³ alpha-cyano-4-hydroxycinnamic acid (CHCA) matrix prepared in solution of acetonitrile and water (1:1; (v/v)). Prepared samples were placed onto the MALDI plate and dried. Samples were analyzed using the MALDI-TOF/TOF

mass spectrometer (4800 MALDI-TOF/TOF™ Analyzer, Applied Biosystems, USA), working in positive reflector mode. In MS analysis, 1600 shots were taken per spectrum, while 2000 shots were acquired in MS/MS analysis, covering the mass range of 900–4000 Da, focus mass 2000 Da, and delay time 450 ns.

For protein identification, we applied the global protein server explorer software (version 3.6, Applied Biosystems, USA) for Mascot (Matrix Science version 2.1, UK) search against National Center for Biotechnology Information protein database (NCBIprot, (RefSeq-release81, March 6, 2017; 31 208 765 769 amino acids, 81 027 309 proteins; Taxonomy Viridiplantae (Green plants) 12.4 million proteins; <http://www.ncbi.nlm.nih.gov/protein>). For combined MS and MS/MS database searches, we used monoisotopic peptide masses with the following search parameters: MS/MS mass fragment tolerance 0.5 Da, mass precursor tolerance 0.3 Da, a maximum of one incomplete cleavage per peptide, peptide charge + 1. All searches were evaluated based on the significant scores obtained from Mascot. Significant threshold value was $P < 0.03$ and FDR value was 2.5%. Universal Protein Resource (UniProt) was used for Gene ontology (GO, <http://www.geneontology.org>) analysis for all identified proteins.

Results

AgNPs stability

TEM analysis of AgNP stock solution revealed the presence of spherical AgNPs (Fig. S1a), which is in accordance with manufacturer's data. Electron dispersive X-ray (EDX) analysis confirmed that detected particles contained silver (Fig. S1b and c).

Spectrophotometric characterization of the exposure solution, i.e., 100 μM AgNP solution in Milli-Q® water during 7 days, showed stable SPR peak at 424 nm (in accordance with manufacturer's data), which remained at the same wavelength until the 7th day, when it slightly increased to 426 nm (Fig. S2a). However, the gradual decrease of absorbance was observed after the 2nd, the 5th, and the 7th day, indicating some instability. Therefore, additional analyses have been made and results are summarized in Fig S2b. A decrease of hydrodynamic diameter was obtained with prolonged exposure, which can indicate smaller particles due to Ag^+ dissociation. ζ potential values became less negative with time, which might suggest that AgNPs lost some of their negatively charged citrate coatings, which favored dissociation of Ag^+ ions. Silver concentration determined after centrifugal ultrafiltration showed that silver dissociation in exposure solution increased during the 7-day period, but did not exceed 1%.

AgNP localization and Ag content in plant tissue

In root cells, AgNPs were visible as black dots (Fig. S3a), which TEM-EDX confirmed as particles containing silver (Fig. S3b and c), proving the direct uptake of AgNPs and their accumulation in the root cells. In the leaf cells, AgNPs could not be detected.

Roots of tobacco plants exposed to either AgNPs or AgNO₃ exhibited a significant increase in Ag uptake of similar values, 1.660 ± 0.051 and 1.617 ± 0.048 mg g⁻¹ DW, respectively. Ag uptake in leaf tissue was significantly lower compared to roots, 0.041 ± 0.004 mg g⁻¹ DW for AgNP treatment and 0.044 ± 0.005 mg g⁻¹ DW for AgNO₃ treatment, respectively.

Differential abundance of root and leaf proteins revealed by 2-DE

For each tissue and treatment, triplicate 2-D gels were obtained from three independent experiments. Representative gels of the proteins from roots of control plants and roots from plants exposed to AgNP or AgNO₃ as well as from leaves of control plants and leaves from plants treated with AgNP or AgNO₃ are shown in Figs. 1 and 2, respectively. Protein spots showing significant and at least 1.5-fold change in abundance between control and treatments were subjected to mass spectrometry analysis.

In root tissue, 44 protein spots showed significant difference in abundance between control and treatments with either AgNPs or AgNO₃ (Fig. 1). Ten spots (1, 3, 4, 5, 7, 32, 25, 29, 43, and 44) could not be identified, while 34 spots were identified as 29 proteins, among which majority was down-regulated (Fig. 3a, Table 1). After exposure to AgNPs, 29 root proteins showed differential abundance, out of which 6 proteins were up-regulated, while 23 exhibited reduced abundance. Treatment with AgNO₃ induced changes in abundance of 26 proteins, out of which 7 exhibited enhanced abundance, while 19 proteins were down-regulated compared to the control (Fig. 3a). A high overlap of differently abundant proteins between AgNP exposure and AgNO₃ exposure was found in roots; 19 proteins were down-regulated, while 6 proteins were up-regulated by both treatments. Only 4 out of 29 proteins had different abundance level between treatments, among which 3 exhibited decreased level only after exposure to AgNPs, while one was down-regulated by AgNPs but up-regulated by AgNO₃ (Fig. 3a, Table 1).

Leaves exhibited 47 protein spots with significant difference in abundance between control and treatments with either AgNPs or AgNO₃ (Fig. 2), among which 7 spots could not be identified (41, 42, 43, 44, 45, 46, and 47). Forty protein spots were identified as 35 proteins and majority of them were down-regulated (Fig. 3b, Table 2). Namely, 27 out of 32 AgNP-responsive proteins identified in leaves were down-

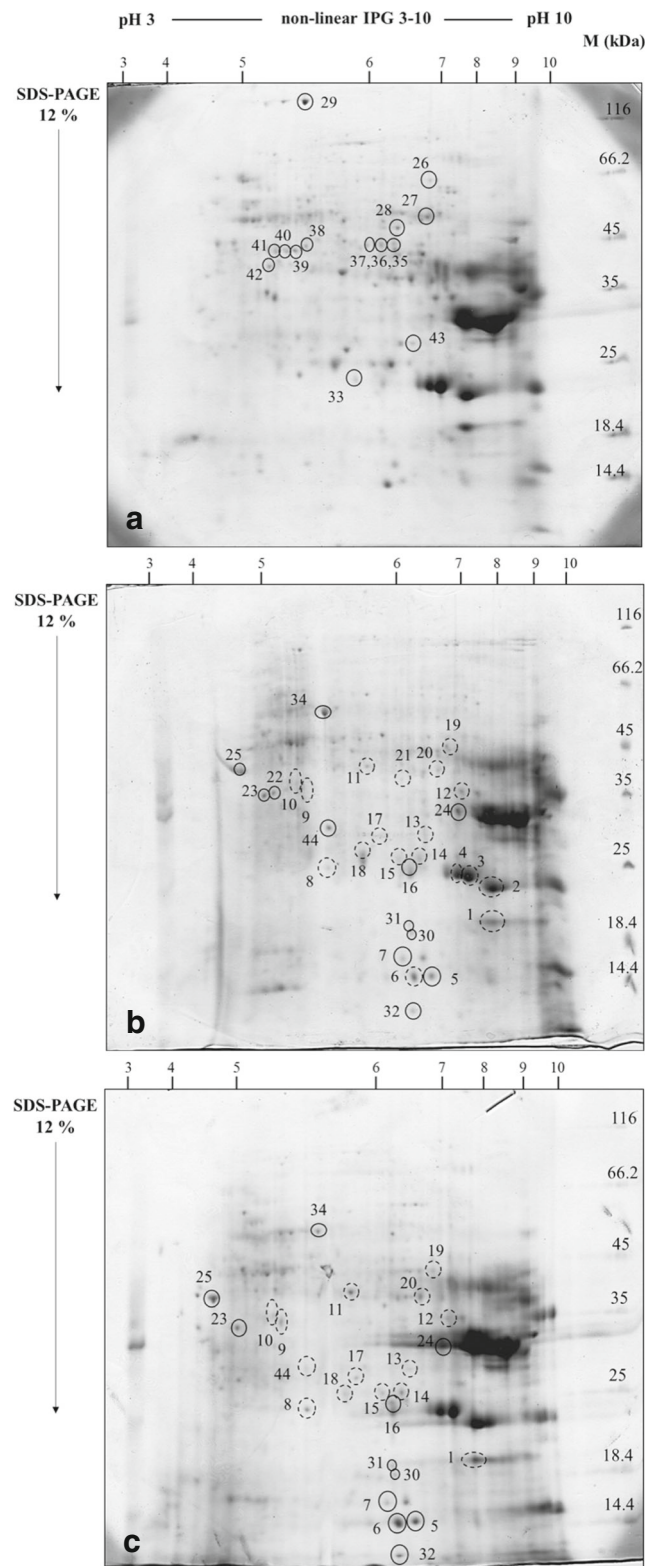


Fig. 1 2-DE analysis of root proteins. Proteome profiles of control roots (a) and roots of tobacco plants treated with either 100 μM AgNPs (b) or 100 μM AgNO₃ (c) were compared. Differently abundant proteins (at least 1.5-fold compared to the control) are indicated by circles; up-regulated proteins are indicated by black line, while down-regulated proteins are indicated with broken-lined circles. The numbers correspond to the numbers listed in Table 1. M, molecular weight markers

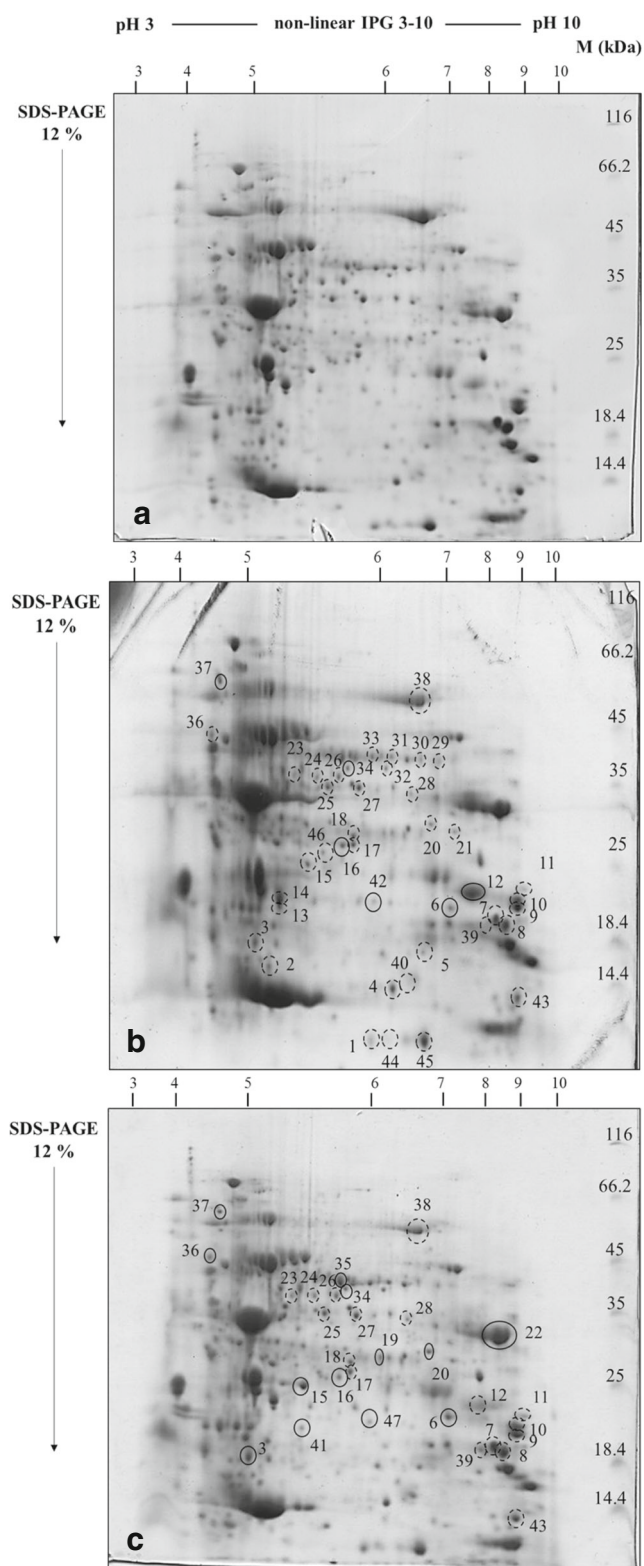


Fig. 2 2-DE analysis of leaf proteins. Proteome profiles of control leaves (a) and leaves of tobacco plants treated with either 100 μM AgNPs (b) or 100 μM AgNO₃ (c) were compared. Differently abundant proteins (at least 1.5-fold compared to the control) are indicated by circles; up-regulated proteins are indicated by black line, while down-regulated proteins are indicated with broken-lined circles. The numbers correspond to the numbers listed in Table 2. M, molecular weight markers

regulated, while the same treatment resulted in up-regulation of only 5 proteins. Treatment with AgNO₃ induced changes in abundance of 25 proteins, out of which 11 proteins were up-regulated and 14 proteins were down-regulated (Fig. 3b). Contrary to root, more than a half (18 out of 35) of the identified proteins exhibited different abundance level between AgNPs and AgNO₃ exposure, among which 3 of them were up-regulated only by AgNO₃ while 4 proteins were also up-regulated by AgNO₃ but down-regulated after AgNP-exposure. Moreover, 10 proteins were repressed by AgNPs, but were not responsive to treatment with AgNO₃ while 1 protein was down-regulated by AgNO₃, but had increased abundance after AgNP treatment (Table 2, Fig. 3b). Among overlapping proteins, 13 had lower abundance and only 4 proteins increased abundance after both treatments (Fig. 3b).

Classification and abundance pattern analysis of root proteins

The detailed information on root protein identification is given in Table S1. Root proteins were classified into 6 functional categories (Fig. 4a and b, Table 1), among which the defense and stress response was the most abundant one. Namely, out of 29 identified root proteins, 16 were ascribed to this category, in which 11 proteins were down-regulated and 4 were up-regulated after both types of treatments; one protein was down-regulated only after exposure to AgNPs (Table 1). Majority of these proteins are involved in response to abiotic and biotic stimuli and response to oxidative stress; they are either pathogenesis-like proteins or perform oxidoreductase activity and are mostly located in extracellular region or vacuole (Fig. 5, Table 1).

Carbohydrate and energy metabolism category was represented with 8 proteins, among which 6 proteins exhibited lower abundance, while one protein was up-regulated after exposure to either AgNPs or AgNO₃; one protein was down-regulated only after exposure to AgNPs (Table 1). Proteins from this category are mostly involved in either mitochondrion-related energy reactions (tricarboxylic acid cycle and ATP synthesis; 3 proteins) or cytosol-related glycolysis (3 proteins) and mostly have oxidoreductase activity (Fig. 5, Table 1).

Two proteins were ascribed to amino acid metabolism category; one, involved in amino acid metabolic process in mitochondrion, was down-regulated by both types of treatments, while the other protein, which participates in glutamine biosynthetic process in cytosol, exhibited lower abundance only after exposure to AgNPs (Fig. 5, Table 1).

Nucleotide metabolism and protein synthesis and processing categories were represented by only one member; protein involved in nucleotide metabolism was down-regulated with AgNP treatment and up-regulated with AgNO₃ treatment, while the translation elongation factor Tu (EF Tu), involved

Table 1 List of differentially abundant proteins in roots of tobacco plants treated with 100 µM AgNPs and 100 µM AgNO₃ with the respect to the control identified by MALDI-TOF/TOF MS/MS and Mascot search against NCBIpro and Uniprot database

Protein accession no. ^a	Species ^b	Score ^c	Mass (Da) ^d	pI ^e	Spots no. ^f	BLASTp <i>N. tabacum</i> protein accession no. ^g	Biological process ^h	Molecular function ⁱ	Cellular compartment ^j	Differential expression ^k
Carbohydrate and energy metabolism										
Putative mitochondrial malate dehydrogenase AAT42189.1	<i>Nicotiana tabacum</i>	199, 180	22,037	7.64	11, 21	–	Tricarboxylic acid cycle	Oxidoreductase activity	Mitochondrion	AgNP ↓ AgNO ₃ =
Isocitrate dehydrogenase AEL48182.1	<i>Capsicum annuum</i>	157, 125	46,706	6.74	36, 37	Predicted: Isocitrate dehydrogenase [NADP]-like XP_016443611.1	Tricarboxylic acid cycle	Oxidoreductase activity	Mitochondrion	AgNP ↓ AgNO ₃ ↓
Triose phosphate isomerase cytosolic isoform-like ABB02628.1	<i>Solanum tuberosum</i>	199	27,012	5.73	17	Triosephosphate isomerase, cytosolic-like NP_001312678.1	Glycolytic process	Isomerase activity	Cytosol	AgNP ↓ AgNO ₃ ↓
Glyceraldehyde 3-phosphate dehydrogenase ABV02033.1	<i>Nicotiana langsdorffii</i> × <i>Nicotiana sanderae</i>	171	37,021	6.62	20	Predicted: Glyceraldehyde-3-phosphate dehydrogenase, cytosolic XP_016498743.1	Glycolytic process	Oxidoreductase activity	Cytosol	AgNP ↓ AgNO ₃ ↓
Enolase NP_001234080.1	<i>Solanum lycopersicum</i>	114	47,798	5.68	34	Enolase NP_001312148.1	Glycolytic process	Lyase activity	Cytosol	AgNP ↑ AgNO ₃ ↑
Predicted: Probable ATP synthase 24-kDa subunit, mitochondrial XP_004253261.1	<i>Solanum lycopersicum</i>	136	27,713	8.69	13	Predicted: Probable ATP synthase 24-kDa subunit, mitochondrial XP_016487066.1	ATP synthesis-coupled proton transport	Proton-transporting ATP synthase activity	Mitochondrion	AgNP ↓ AgNO ₃ ↓
Glycosyl hydrolase family 38 protein isoform 5 XP_007038136.1	<i>Theobroma cacao</i>	95	86,807	6.48	26	Predicted: Alpha-mannosidase XP_016465882.1	Carbohydrate metabolic process	Glycosidase activity	ER Golgi complex	AgNP ↓ AgNO ₃ ↓
ADH-like UDP-glucose dehydrogenase AAT40104.1	<i>Nicotiana tabacum</i>	159	41,177	6.20	35	–	Carbohydrate metabolic process	Oxidoreductase activity	Cytosol	AgNP ↓ AgNO ₃ ↓
Defense and stress response										
Pathogen- and wound-inducible antifungal protein CBP20 precursor AAB29959.2	<i>Nicotiana tabacum</i>	75, 80	22,168	8.39	31	–	Response to abiotic and biotic stimuli	Pathogenesis-related protein	Vacuole	AgNP ↑ AgNO ₃ ↑
Basic beta-1,3-glucanase ACF93731.1	<i>Nicotiana tabacum</i>	103	40,391	7.10	24	–	Response to abiotic and biotic stimuli	Pathogenesis-related protein	Vacuole	AgNP ↑ AgNO ₃ ↑
CAP, cysteine-rich secretory protein, antigen 5 XP_003593367.1	<i>Medicago truncatula</i>	80	18,287	9.25	30	Predicted: Basic form of pathogenesis-related protein 1-like XP_016442988.1	Response to abiotic and biotic stimuli	Pathogenesis-related protein	Extracellular region	AgNP ↑ AgNO ₃ ↑
Osmotin AAB23375.1	<i>Nicotiana tabacum</i>	111	26,681	8.13	2	–	Response to abiotic and biotic stimuli	Pathogenesis-related protein	Vacuole	AgNP ↓ AgNO ₃ =
Rhoadhesin receptor precursor, putative XP_002531991.1	<i>Ricinus communis</i>	129	21,177	8.74	14	Predicted: Germin-like protein subfamily 1 member 20 XP_016470784.1	Response to abiotic and biotic stimuli	Pathogenesis-related protein	Extracellular region	AgNP ↓ AgNO ₃ ↓
Rhoadhesin receptor precursor, putative XP_002511486.1	<i>Ricinus communis</i>	75	23,441	6.64	15	Predicted: Germin-like protein subfamily 1 member 2 XP_016499460.1	Response to abiotic and biotic stimuli	Pathogenesis-related protein	Extracellular region	AgNP ↓ AgNO ₃ ↓
Germin-like protein subfamily 1 member 20 precursor AFW90592.1	<i>Solanum tuberosum</i>	97	24,399	6.49	18	Predicted: Putative germin-like protein 2-1 XP_016455584.1	Response to abiotic and biotic stimuli	Pathogenesis-related protein	Extracellular region	AgNP ↓ AgNO ₃ ↓
Annexin CAA75214.1	<i>Nicotiana tabacum</i>	201	35,950	5.38	10	–	Response to abiotic and biotic stimuli	Calcium-dependent phospholipid binding	Cytosol	AgNP ↓ AgNO ₃ ↓
Vacuole-associated annexin VCaB42 AAD24540.1	<i>Nicotiana tabacum</i>	81	35,938	5.34	9	–	Response to abiotic and biotic stimuli	Calcium-dependent phospholipid binding	Vacuole	AgNP ↓ AgNO ₃ ↓
Iron superoxide dismutase AHG12637.1	<i>Nicotiana tabacum</i>	85	28,338	8.60	8	–	Response to oxidative stress	Oxidoreductase activity	Plastid	AgNP ↓ AgNO ₃ ↓
Manganese superoxide dismutase BAC75399.1	<i>Nicotiana tabacum</i>	78	20,878	6.36	16	–	Response to oxidative stress	Oxidoreductase activity	Mitochondrion	AgNP ↑ AgNO ₃ ↑
Predicted: Subunitization-associated anionic peroxidase 2-like XP_006343273.1	<i>Solanum tuberosum</i>	89	36,319	6.32	12	Predicted: Peroxidase XP_016472675.1	Response to oxidative stress	Oxidoreductase activity	Extracellular region	AgNP ↓ AgNO ₃ ↓

Table 1 (continued)

Protein accession no. ^a	Species ^b	Score ^c	Mass (Da) ^d	pI ^e	Spots no. ^f	BLASTp <i>N. tabacum</i> protein accession no. ^g	Biological process ^h	Molecular function ⁱ	Cellular compartment ^j	Differential expression ^k
Salicylic acid binding catalase, partial AAC48918.1	<i>Nicotiana tabacum</i>	198	56,824	6.60	27	–	Response to oxidative stress	Oxidoreductase activity	Peroxisome	AgNP ↓ AgNO ₃ ↓
Monodehydroascorbate reductase AGX01486.1	<i>Nicotiana tabacum</i>	326	52,056	8.09	28	–	Response to oxidative stress	Oxidoreductase activity	Cytosol Mitochondrion Plastid	AgNP ↓ AgNO ₃ ↓
Monodehydroascorbate reductase ABF5909.1	<i>Rheum australe</i>	123, 126, 87	47,325	5.63	38, 40, 41	Predicted: Monodehydroascorbate reductase XP_016455903.1	Response to oxidative stress	Oxidoreductase activity	Cytosol	AgNP ↓ AgNO ₃ ↓
Quinone reductase, partial BAK53859.1	<i>Nicotiana benthamiana</i>	78	21,242	5.82	33	Predicted: Probable NAD(P)H dehydrogenase (quinone) FQR1-like I XP_016435124.1	Response to oxidative stress	Oxidoreductase activity	Plasma membrane	AgNP ↓ AgNO ₃ ↓
Protein synthesis and processing Predicted: Elongation factor Tu, mitochondrial XP_004136065.1	<i>Cucumis sativus</i>	115	48,845	6.58	39	Predicted: Elongation factor Tu, mitochondrial XP_016494694.1	Protein biosynthesis	Translation elongation factor activity	Mitochondrion	AgNP ↓ AgNO ₃ ↓
Amino acid metabolism										
Glutamate dehydrogenase CAD12373.1	<i>Nicotiana tabacum</i>	122	44,588	6.57	19	–	Cellular amino acid metabolic process	Oxidoreductase activity	Mitochondrion	AgNP ↓ AgNO ₃ ↓
Glutamine synthetase GS56 AAR86718.1	<i>Nicotiana attenuata</i>	213	39,192	5.81	42	Predicted: glutamine synthetase cytosolic isozyme 1-1 XP_016466322.1	Glutamine biosynthetic process	Ligase activity	Cytosol	AgNP ↓ AgNO ₃ ↓ AgNO ₃ =
Nucleotide metabolism										
Nucleoside diphosphate kinase NP_001234174	<i>Solanum lycopersicum</i>	201	16,252	6.30	6	Nucleoside diphosphate kinase 1 XP_016467992.1	Nucleotide metabolism	Transferase activity	Nucleus Cytosol Peroxisome	AgNP ↓ AgNO ₃ ↑
Unknown Predicted: Outer membrane protein A-like XP_004153053.1	<i>Cucumis sativus</i>	247, 131	–	–	22, 23	–	–	–	–	AgNP ↑ AgNO ₃ ↑

^a Protein accession number according to NCBIprote

^b Plant species according to Mascot search result and NCBIprote database

^c The highest score obtained by Mascot search result according to NCBIprote database

^d Theoretical mass according to Uniprot database

^e Theoretical isoelectric point according to Uniprot database

^f Spot number corresponds to the 2-DE gels presented in Fig. 1

^g Protein accession number according to NCBIprote obtained after BLASTp alignment

^h Biological process was derived through Uniprot hit accessions for all identified proteins

ⁱ Molecular function was derived through Uniprot hit accessions for all identified proteins

^j Cellular compartment was derived through Uniprot hit accessions for all identified proteins

^k Differential expression of protein spots if the spot volume is at least 1.5× higher (↑) or 1.5× lower (↓) compared to the control or of equal volume (=)

Amino acid metabolism category was represented with two proteins (Table 2), protein which was down-regulated with AgNPs and up-regulated with AgNO₃ participates in glycine catabolic process and is located in mitochondrion. The other one, which exhibited lower abundance only after the treatment with AgNPs, is engaged in glutathione metabolic process as well as in response to oxidative stress and is located in cytosol (Fig. 6, Table 2).

Nucleoside diphosphate kinase 1 was the only protein of the nucleotide metabolism category and was down-regulated only after exposure to AgNPs. Beside nucleotide metabolism, this protein is also involved in stress response and can be found in nucleus, cytosol, and peroxisome (Fig. 6, Table 2).

Two proteins were assigned to the unknown category (Fig. 6, Table 2).

PCA analysis identified differences in protein abundance patterns between control and treatments with AgNPs and AgNO₃ (Fig. S4b). Proteins related to PC1 (positive direction) mostly belonged to the carbohydrate and energy metabolism as well as to the defense and stress response (CBP20 and glutathione S-transferase (GST)), protein synthesis and processing (peptidyl-prolyl cis-trans isomerase), RNA processing (glycine-rich RNA-binding protein (GRP), and mRNA-binding protein (mRBP)), nucleotide metabolism (NDPK1), and protein with unknown function (elicitor inducible), which were all more abundant in control plants. Proteins related to PC1 (negative direction) were partial Rubisco large subunit (RbcL) and chlorophyll *a-b*-binding protein (carbohydrate and energy metabolism), protease Do-like (protein synthesis and processing) and the unknown protein At5g39570-like, which were all more abundant in plants exposed to both types of treatments. In PC2 (positive direction), we found ATP synthase 24-kDa subunit, Rubisco activase, and beta-carbonic anhydrase (carbohydrate and energy metabolism); iron superoxide dismutase (Fe-SOD), β -1,3-glucanase, and ankyrin-repeat-containing protein (defense and stress response); and aminomethyltransferase (amino acid metabolism) that increased in AgNO₃-treated plants. In PC2 (negative direction), we found osmotin (defense and stress response) that increased after AgNP treatment (Fig. S4b).

Discussion

Proteins are directly involved in stress response both as structural proteins and also as proteins engaged in regulation of plant epigenome, transcriptome and metabolome (Kosová et al. 2018). Therefore, studies of changes in protein abundance during stress induction can provide important information on how plants cope with stress factors. Proteomic-based studies on plant responses to AgNP-induced stress employed so far show that in rice, AgNPs interact with normal cell metabolic processes, such as protein synthesis/degradation and

apoptosis (Mirzajani et al. 2014), while in wheat seedlings, AgNPs altered abundance of proteins involved in primary metabolism and cell defense (Vannini et al. 2014). Only two studies have compared changes in plant proteomes after simultaneous exposure to AgNPs and AgNO₃. In the study conducted on *Eruca sativa* (rocket), it was found that both Ag treatments cause changes in proteins involved in the redox regulation and in the sulphur metabolism (Vannini et al. 2013); however, the low level of overlap of differently abundant proteins was found between AgNPs and AgNO₃ treatments, suggesting specific nanoparticles effects. On the other hand, in tobacco seedlings, it was found that majority of identified proteins exhibited similar abundance response after both treatments, thus indicating that dissociated Ag⁺ ions could be involved in AgNP toxicity (Peharec Štefanić et al. 2018).

In this study, a high overlap of differently abundant proteins between AgNP and AgNO₃ treatments was found in tobacco roots, but in leaf tissue, almost a half of the proteins exhibited different abundance level between AgNP exposure and AgNO₃ exposure. A schematic comparison of protein abundance in the roots and leaves of tobacco adult plant in response to exposure to 100 μ M AgNPs or 100 μ M AgNO₃ has been generated (Fig. 7). Obtained results indicate that AgNPs and AgNO₃ cause similar changes in the root proteome, but more distinct changes in the proteome of the leaf cells, although in both tissues, higher suppression of protein abundance was induced by AgNPs. Several proteins in roots, such as osmotin, NDPK1, and GS, were decreased only by AgNP treatment. These data confirm evidences found in other organisms (Domingos et al. 2011; Poynton et al. 2012) that AgNP effects on the gene expression patterns are not only due to the dissociated Ag⁺ ions. Interestingly, only several proteins (osmotin, basic beta-1,3-glucanase, CBP20, Fe-SOD, glyceraldehyde-3-phosphate dehydrogenase (GAPDH), triose phosphate isomerase (TPI), and MDH) were found to be regulated by silver treatments in both tobacco tissues. This tissue-dependent response probably results from differences in metal content, as silver accumulation in roots was several times higher than in leaves, after both types of treatments. Tissue-specific response has not been extensively studied so far, although reports on metal-induced stress show that proteins in roots and leaves are differently regulated by exposure to cadmium, generating different detoxification mechanisms (Lee et al. 2010).

Root proteome

Majority of the identified proteins in roots were those involved in defense and stress response. Given that the roots were the first in contact with the investigated treatments and that silver largely accumulated in the root after exposure to both AgNPs and AgNO₃, these findings could be associated with (nano)silver-imposed stress. We identified several

Table 2 List of differentially abundant proteins in leaves of tobacco plants treated with 100 μM AgNPs and 100 μM AgNO₃ with the respect to the control identified by MALDI-TOF/TOF MS/MS and Mascot search against NCBIpro and Uniprot database

Protein accession no. ^a	Species ^b	Score ^c	Mass (Da) ^d	pI ^e	Spots no. ^f	BLASTp <i>N. tabacum</i> protein accession no. ^g	Biological process ^h	Molecular function ⁱ	Cellular compartment ^j	Differential expression ^k
Carbohydrate and energy metabolism										
Photosystem II 11-kD protein NP_001147626.1	<i>Zea mays</i>	114	17,359	9.98	1	Predicted: photosystem II repair protein PSB27-H1, chloroplastic-like XP_016514812.1	Photosynthesis	Photosystem II assembly	Chloroplast	AgNP ↓ AgNO ₃ =
PSI-E1 = 14.4-kDa photosystem I psaE product {N-terminal} AAB29519.1	<i>Nicotiana tabacum</i>	96	n. p.	n. p.	7	-	Photosynthesis	Protein domain specific binding	Chloroplast	AgNP ↓ AgNO ₃ ↓
PSI-E subunit of photosystem I BAA07667.1	<i>Nicotiana sylvestris</i>	130	15,224	9.74	8	Predicted: Photosystem I reaction center subunit IV B, chloroplastic XP_016496470.1	Photosynthesis	Protein domain specific binding	Chloroplast	AgNP ↓ AgNO ₃ ↓
Photosystem I reaction center subunit II, chloroplastic EMS56878.1	<i>Triticum urartu</i>	130	17,704	9.77	9	Predicted: Photosystem I reaction center subunit II, chloroplastic-like XP_016505719.1	Photosynthesis	Protein domain specific binding	Chloroplast	AgNP ↓ AgNO ₃ ↓
PSI-D1 precursor BAA02871.1	<i>Nicotiana sylvestris</i>	145	23,456	9.84	10	Photosystem I reaction center subunit II, chloroplastic-like XP_016455922.1	Photosynthesis	Protein domain specific binding	Chloroplast	AgNP ↓ AgNO ₃ ↓
23-kDa polypeptide of photosystem II oxygen-evolving complex CAA44292.1	<i>Nicotiana tabacum</i>	325, 306	28,378	7.63	13, 14	-	Photosynthesis	Calcium-ion binding	Chloroplast	AgNP ↓ AgNO ₃ =
Predicted: Chlorophyll <i>a-b</i> -binding protein 8, chloroplastic-like XP_004251826.1	<i>Solanum lycopersicum</i>	75	29,278	8.61	16	Predicted: Chlorophyll <i>a-b</i> -binding protein 8, chloroplastic-like XP_016457506.1	Photosynthesis	Chlorophyll binding	Chloroplast	AgNP ↑ AgNO ₃ ↑
Predicted: Ferredoxin-NADP reductase, leaf-type XP_006340740.1	<i>Solanum tuberosum</i>	247, 174	40,457	8.37	25, 27	Predicted: Ferredoxin-NADP reductase, leaf-type isozyme, chloroplastic XP_016433650.1	Photosynthesis	Oxidoreductase activity	Chloroplast	AgNP ↓ AgNO ₃ ↓
Ribulose-1,5-bisphosphate carboxylase/oxygenase large subunit, partial ABP82410.1	<i>Ulva pertusa</i>	75	43,780	6.18	6	Ribulose-1,5-bisphosphate carboxylase/oxygenase large subunit NP_054507.1	Photosynthesis Photorespiration	Oxidoreductase activity	Chloroplast	AgNP ↑ AgNO ₃ ↑
Ribulose-1,5-bisphosphate carboxylase/oxygenase large subunit AAD15025.1	<i>Nicotiana tabacum</i>	369	52,898	6.41	38	-	Photosynthesis Photorespiration	Oxidoreductase activity	Chloroplast	AgNP ↓ AgNO ₃ ↓
Ribulose biphosphate carboxylase/oxygenase activase 2 (chloroplast) AFB70996.1	<i>Nicotiana attenuata</i>	104	48,283	7.58	35	Predicted: Ribulose biphosphate carboxylase/oxygenase activase 2, chloroplastic-like XP_016477286.1	Photosynthesis	ATP binding	Chloroplast	AgNP = AgNO ₃ ↑
ATP synthase CF1 epsilon subunit NP_054505.1	<i>Nicotiana tabacum</i>	103	14,607	5.18	3	-	ATP synthesis-coupled proton transport	Proton-transporting ATP synthase activity	Chloroplast	AgNP ↓ AgNO ₃ ↑
Predicted: Ribulose-phosphate 3-epimerase, chloroplastic-like XP_006364582.1	<i>Solanum tuberosum</i>	84	30,342	7.72	17	Predicted: Ribulose-phosphate 3-epimerase, chloroplastic XP_016514719.1	Carbohydrate metabolic process	Racemase and epimerase activity	Chloroplast	AgNP ↓ AgNO ₃ ↓
Beta-carbonic anhydrase AAL51055.2	<i>Nicotiana tabacum</i>	82	34,452	6.19	19	-	Carbohydrate metabolic process	Lyase activity	Plasma membrane	AgNP = AgNO ₃ ↑
Putative mitochondrial malate dehydrogenase AAT42189.1	<i>Nicotiana tabacum</i>	98	22,037	7.64	32	-	Tricarboxylic acid cycle	Oxidoreductase activity	Mitochondrion	AgNP ↓ AgNO ₃ =

Table 2 (continued)

Protein accession no. ^a	Species ^b	Score ^c	Mass (Da) ^d	pI ^e	Spots no. ^f	BLASTp <i>N. tabacum</i> protein accession no. ^g	Biological process ^h	Molecular function ⁱ	Cellular compartment ^j	Differential expression ^k
Triose phosphate isomerase cytosolic isoform-like ABB02628.1	<i>Solanum tuberosum</i>	225	27,012	5.73	18	Triosephosphate isomerase NP_001312678.1	Glycolytic process	Isomerase activity	Cytosol	AgNP ↓ AgNO ₃ ↓
Glyceraldehyde-3-phosphate dehydrogenase CAB39974.1	<i>Nicotiana tabacum</i>	144, 137	36,725	7.70	29, 30	–	Glycolytic process	Oxidoreductase activity	Cytosol	AgNP ↓ AgNO ₃ =
Plastidic aldolase ADE74633.1	<i>Nicotiana tabacum</i>	276	42,806	6.38	23	–	Glycolytic process	Lyase activity	Chloroplast	AgNP ↓ AgNO ₃ ↓
Plastidic aldolase NPALDP1 BAA77604.1	<i>Nicotiana paniculata</i>	331, 410	42,574	6.92	24, 26	Predicted: Fructose-bisphosphate aldolase 1, chloroplastic XP_016505617.1	Glycolytic process	Lyase activity	Chloroplast	AgNP ↓ AgNO ₃ ↓
Defense and stress response										
Pathogen- and wound-inducible antifungal protein CBP20 precursor AAB29959.2	<i>Nicotiana tabacum</i>	131	22,168	8.39	11	–	Response to abiotic and biotic stimuli	Pathogenesis-related protein	Vacuole	AgNP ↓ AgNO ₃ ↓
CBP20 AAB29960.1	<i>Nicotiana tabacum</i>	131	21,922	8.40	39	–	Response to abiotic and biotic stimuli	Pathogenesis-related protein	Vacuole	AgNP ↓ AgNO ₃ ↓
Basic beta-1,3-glucanase ACF93731.1	<i>Nicotiana tabacum</i>	308	40,391	7.10	22	–	Response to abiotic and biotic stimuli	Pathogenesis-related protein	Vacuole	AgNP = AgNO ₃ =
Osmotin AAB23375.1	<i>Nicotiana tabacum</i>	75	26,681	8.13	12	–	Response to abiotic and biotic stimuli	Pathogenesis-related protein	Vacuole	AgNP ↑ AgNO ₃ ↑
Ankyrin-repeat protein HBP1 AAK18619.1	<i>Nicotiana tabacum</i>	201	37,317	4.45	36	–	Response to abiotic and biotic stimuli	Protein domain specific binding	Chloroplast	AgNP ↓ AgNO ₃ ↓
Iron superoxide dismutase AHG12637.1	<i>Nicotiana tabacum</i>	175	28,338	8.60	15	–	Response to oxidative stress	Oxidoreductase activity	Nucleus Chloroplast	AgNP ↑ AgNO ₃ ↑
RNA processing										
Glycine-rich RNA-binding protein ACD03270.1	<i>Nicotiana tabacum</i>	155	15,652	5.23	2	–	mRNA processing	RNA binding	Nucleus	AgNP ↓ AgNO ₃ =
mRNA-binding protein precursor, partial AAP87140.1	<i>Nicotiana tabacum</i>	92, 107	44,245	6.51	31, 33	–	mRNA processing	RNA binding	Chloroplast	AgNP ↓ AgNO ₃ =
Protein synthesis and processing										
Predicted: Protease Do-like 1, chloroplastic-like XP_006338559.1	<i>Solanum tuberosum</i>	335	45,671	6.45	34	Predicted: Protease Do-like 1, chloroplastic XP_016443403.1	Proteolysis	Peptidase activity	Chloroplast	AgNP ↑ AgNO ₃ ↑
Predicted: 30S ribosomal protein S5, chloroplastic-like XP_004232896.1	<i>Solanum lycopersicum</i>	142	33,372	8.87	28	Predicted: 30S ribosomal protein S5, chloroplastic XP_016507755.1	Translation	RNA binding	Chloroplast	AgNP ↓ AgNO ₃ ↓
Peptidyl-prolyl cis-trans isomerase cyclophilin-type family protein XP_002303772.1	<i>Populus trichocarpa</i>	95	28,565	9.51	5	Peptidyl-prolyl cis-trans isomerase XP_016481087.1	Protein folding	Isomerase activity	Cytosol	AgNP ↓ AgNO ₃ =
Amino acid metabolism										
Predicted: Aminomethyltransferase, mitochondrial-like, XP_004232698.1	<i>Solanum lycopersicum</i>	227	44,294	8.65	20	Predicted: Aminomethyltransferase, mitochondrial XP_016485574.1	Glycine catabolic process	Transferase activity	Mitochondrion	AgNP ↓ AgNO ₃ ↑
Predicted: Glutathione S-transferase-like XP_006342558.1	<i>Solanum tuberosum</i>	85	25,147	6.19	21	Predicted: Putative glutathione S-transferase-like XP_016455705.1	Glutathione metabolic process	Transferase activity	Cytosol	AgNP ↓ AgNO ₃ =
							Response to oxidative stress			

Table 2 (continued)

Protein accession no. ^a	Species ^b	Score ^c	Mass (Da) ^d	pI ^e	Spots no. ^f	BLASTp <i>N. tabacum</i> protein accession no. ^g	Biological process ^h	Molecular function ⁱ	Cellular compartment ^j	Differential expression ^k
Nucleotide metabolism Nucleoside diphosphate kinase I XP_002872441.1	<i>Arabidopsis lyrata subsp. lyrata</i>	121	16,434	6.30	4	Nucleoside diphosphate kinase I XP_016467992.1	Nucleotide metabolism	Transferase activity	Nucleus Cytosol Peroxisome	AgNP ↓ AgNO ₃ =
Unknown Predicted: Uncharacterized protein At5g39570-like XP_006338424.1	<i>Solanum tuberosum</i>	102	40,988	4.66	37	Predicted: Uncharacterized protein At5g39570-like XP_016449031.1	Unknown	–	–	AgNP ↑ AgNO ₃ ↑
Elicitor inducible protein BAB13708.1	<i>Nicotiana tabacum</i>	103	19,579	5.41	40	–	Unknown	–	–	AgNP ↓ AgNO ₃ =

^a Protein accession number according to NCBIprote

^b Plant species according to Mascot search result and NCBIprote database

^c The highest score obtained by Mascot search result according to NCBIprote database

^d Theoretical mass according to Uniprot database

^e Theoretical isoelectric point according to Uniprot database

^f Spot number corresponds to the 2-DE gels presented in Fig. 2

^g Protein accession number according to NCBI obtained after BLASTp alignment

^h Biological process was derived through Uniprot hit accessions for all identified proteins

ⁱ Molecular function was derived through Uniprot hit accessions for all identified proteins

^j Cellular compartment was derived through Uniprot hit accessions for all identified proteins

^k Differential expression of protein spots if the spot volume is at least 1.5× higher (↑) or 1.5× lower (↓) compared to the control or of equal volume (=)

pathogenesis-related (PR) proteins, which are known to accumulate in response to infections by viruses, bacteria, or fungi, but also after treatments with different abiotic stressors, including excess metals (Sudisha et al. 2012). There are at least 17 different PR families and each group consists of several members with similar properties (Sudisha et al. 2012). In our experiment, exposure to AgNPs and AgNO₃ increased abundance of three PR proteins from different families: precursor of protein CBP20 (PR-4 family, chitinase types I and II), CAP protein predicted to be a basic form of pathogenesis-related protein 1 (PR-1 family), and basic β-1,3-glucanase (PR-2 family). CBP20 protein and basic β-1,3-glucanases were found to be induced by heavy metals (Hensel et al. 1999; Su et al. 2016) and although they are expected to be localized in the vacuole, there are reports about their extracellular accumulation (Kunze et al. 1998). Hensel et al. (1999) speculated that stress situations can lead to an accumulation of CBP20 in the cell wall to protect cells against damages caused by wounding and heavy metals. Moreover, it was proposed that basic β-1,3-glucanase, which functions in the regulation of callose at plasmodesmata, can be responsible for resistance to metals as decreased callose levels in response to excess metals and increased plasmodesmatal permeability may lessen the negative effects of metals on primary root growth (O'Lexy et al. 2018). Vannini et al. (2014) reported that PR proteins are the components of the plant response against AgNPs. By TEM-EDX analysis, we confirmed AgNPs accumulation inside the root cells of tobacco plants; thus, up-regulation of abovementioned

Fig. 5 GO analysis of root proteins identified after exposure to 100 μM AgNPs and 100 μM AgNO₃. Differently abundant proteins were identified by MALDI-TOF/TOF MS according to the NCBIprot database. GO analysis was derived through Uniprot hit accessions for all protein identifications according to three categories which describe biological process (a), molecular function (b), and cellular compartment (c)

PR proteins involved in modifications of cell wall can contribute to defense against (nano)silver stress (Kosová et al. 2018). However, three PR proteins, identified as members of germin-like protein (GLP) superfamily, were found to be down-regulated with both types of treatments. These proteins, classified as PR-16 family (Sudisha et al. 2012), are ubiquitously expressed in plants and play important roles in development (Dunwell et al. 2008) and response to stress (Wang et al. 2013). However, down-regulation of certain members of GLPs was also reported after plant exposure to NaCl (Wang et al. 2013). Interestingly, GLPs were the most down-regulated gene family in Arabidopsis roots during biosynthesis of gold nanoparticles, although proteome analysis did not reveal changes in GLP protein levels (Tiwari et al. 2016). It seems that different response, i.e., increased or decreased expression of certain GLPs, could be associated with time- and/or dose-dependent activation (Dunwell et al. 2008). Osmotin, protein which belongs to the PR-5 family, was also down-regulated, but only after exposure to AgNPs. As other PR proteins, osmotin is involved in the modulation of plant responses to

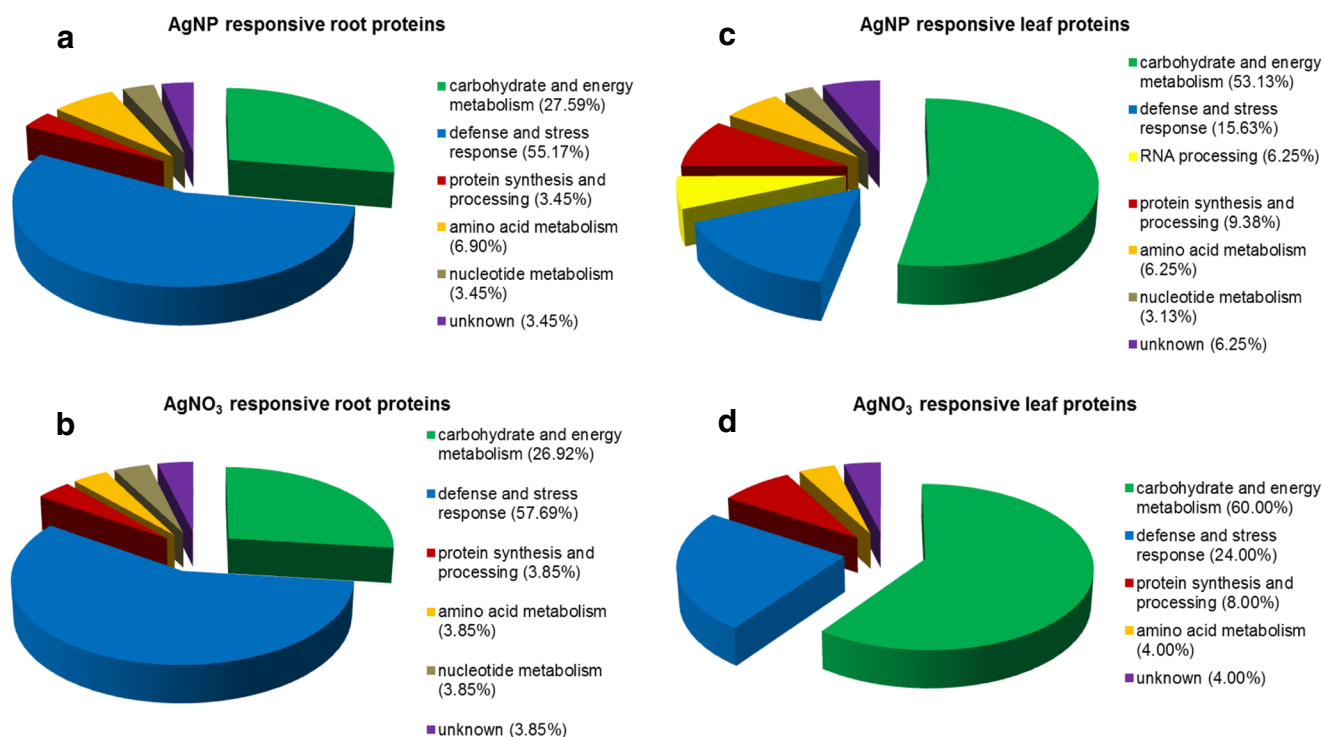
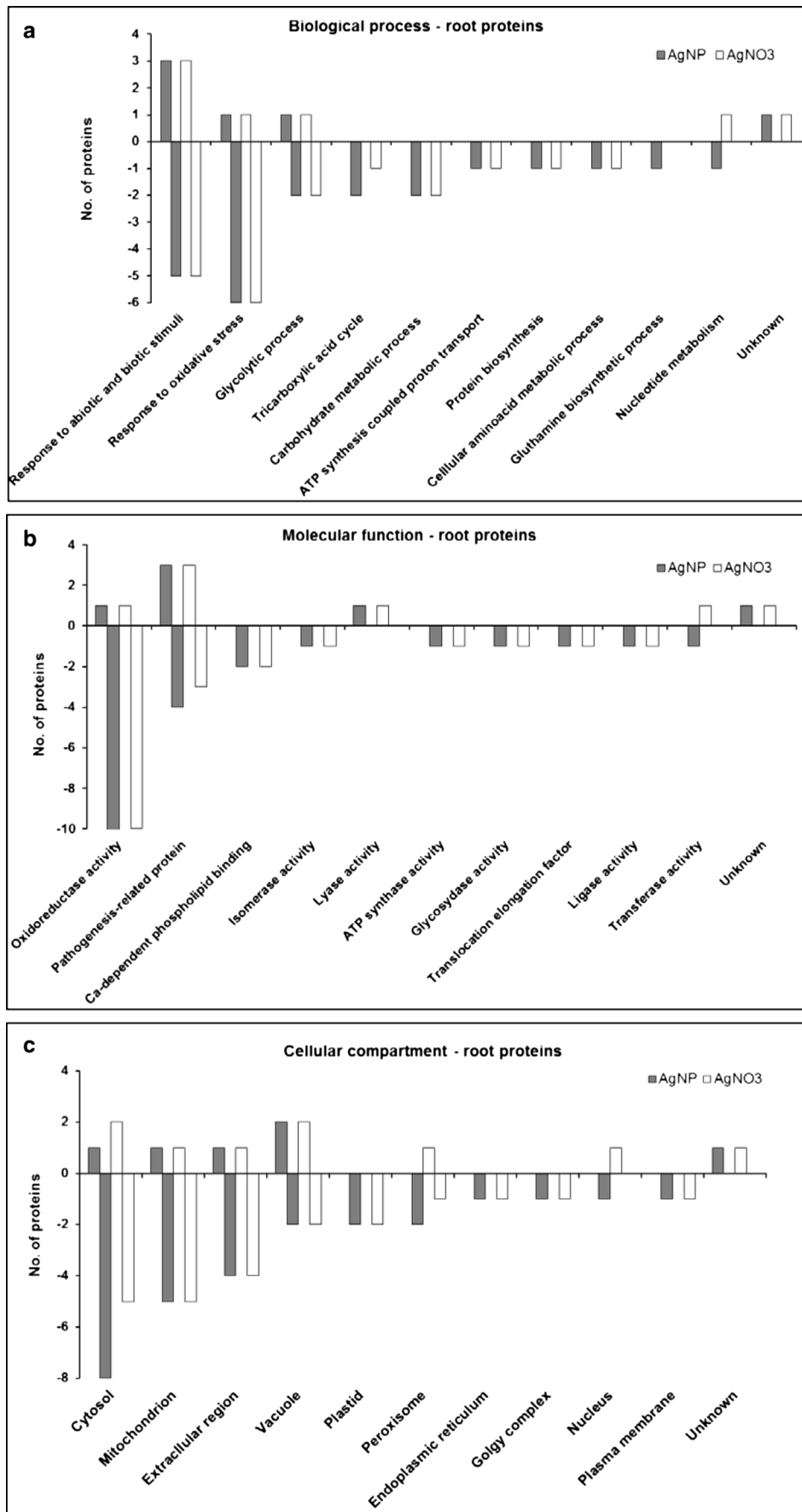
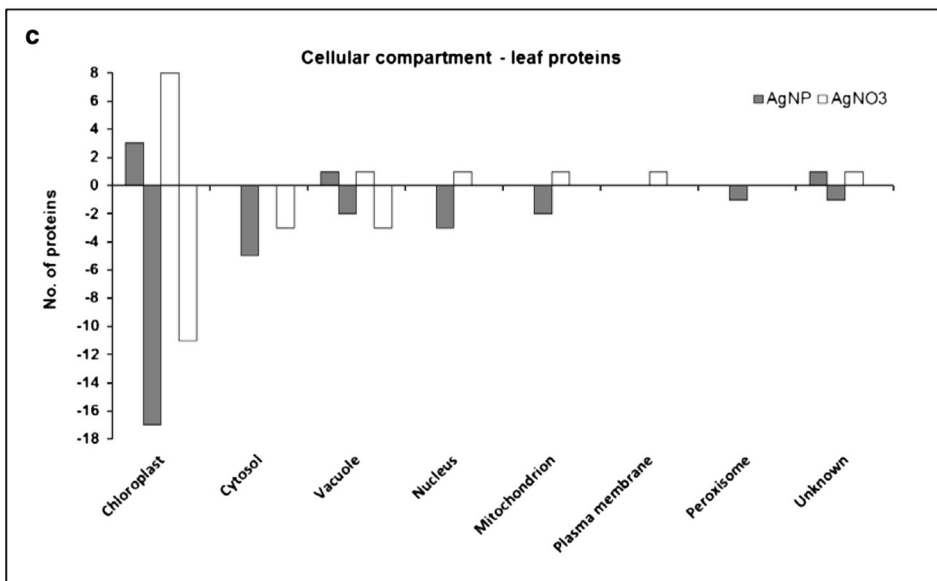
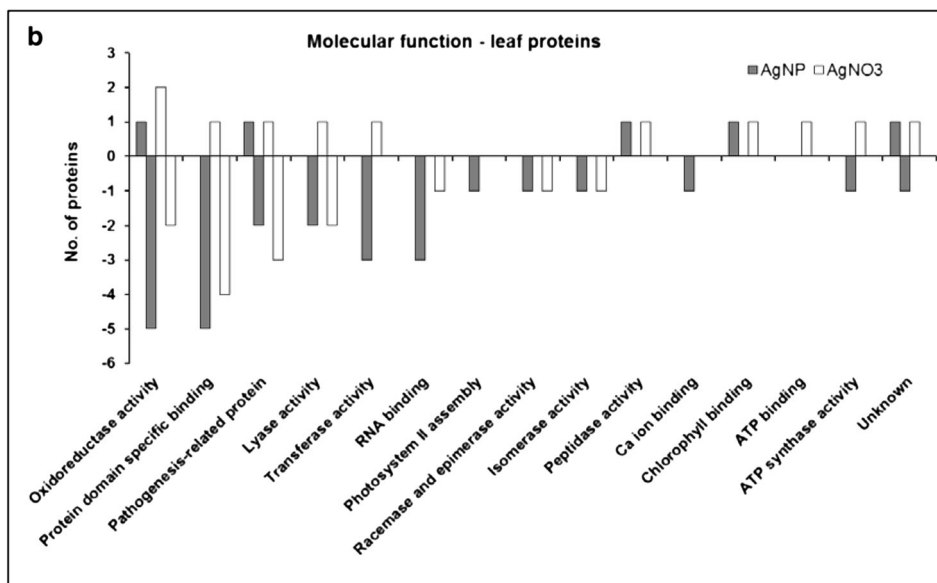
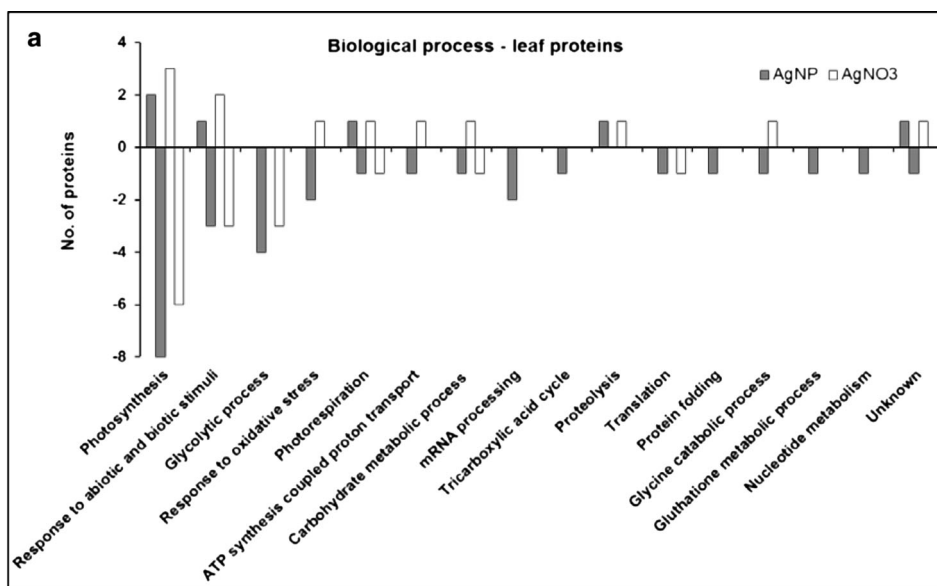


Fig. 4 Functional categorization of the differently abundant proteins in roots (a) and leaves (b) of tobacco plants exposed to 100 μM AgNPs and of differently abundant proteins in roots (c) and leaves (d) of tobacco plants exposed to 100 μM AgNO₃





◀ **Fig. 6** GO analysis of leaf proteins identified after exposure to 100 μM AgNPs or 100 μM AgNO₃. Differently abundant proteins were identified by MALDI-TOF/TOF MS according to the NCBIprot database. GO analysis was derived through Uniprot hit accessions for all protein identifications according to three categories which describe biological process (a), molecular function (b), and cellular compartment (c)

stress (Hakim Ullah et al. 2018) by acting as a transcriptional regulator or a signalling molecule (Sudisha et al. 2012). As presented, the responses of different types of PR proteins during abiotic and biotic stress are very well documented in literature; however, there are still gaps in understanding the exact mechanisms of action during their multiple functions in plant defense.

Annexins are soluble proteins involved in the organization of membrane-associated protein networks which participate in a wide range of cellular and developmental processes, including tolerance to abiotic stress (Laohavisit and Davies 2011). The majority of plant annexins has been localized in the cytosol; however, they have also been found in other cell compartments such as vacuole (Laohavisit and Davies 2011). Two annexins were identified in tobacco roots in this study; one vacuole-associated VCaB42 and the other located in the cytosol, and both were found to be down-regulated in response to AgNPs or AgNO₃. Our findings are in a good correlation with report of Mustafa et al. (2015), in which several cell organization-related proteins, including annexin 8, were down-regulated by AgNPs in soybean roots. Obtained results may indicate stagnant status of root cell division and elongation under stress conditions imposed by AgNPs, as suggested by Mustafa et al. (2015), particularly since the annexin VCaB42 was found to be involved in the expansion of tobacco cells and in the early events of vacuole biogenesis (Seals and Randall 1997).

Among root proteins involved in defense and stress response, several antioxidant enzymes, which serve to detoxify reactive oxygen species (ROS), were identified. Most of the proteomic research on plant response to various stress factors revealed a positive correlation between stress tolerance and an increased abundance of antioxidant proteins (Kosová et al. 2018). However, there are several reports which show that excess metals can lead to decreased expression of antioxidant enzymes (Hossain and Komatsu 2013 and references therein). Fe-SOD, located in plastids, was down-regulated in response to AgNPs or AgNO₃, which is in a good correlation with decreased SOD activity recorded in roots after treatment with 100 μM AgNPs (Cvjetko et al. 2018). However, Mn-SOD, a mitochondrial isoform, was up-regulated after both types of treatments. Root proteome analysis of *Brassica juncea* exposed to Cd revealed up-regulation of Fe-SOD, while Cu/Zn-SOD was down-regulated (Alvarez et al. 2009), suggesting that different SOD genes could play different roles in eliminating ROS. Abundance of other identified antioxidant enzymes, peroxidase, salicylic acid binding catalase,

monodehydroascorbate reductase (MDHAR), and quinone reductase was also decreased after exposure to silver treatments. These findings are in a good correlation with results from our previous study, in which majority of the investigated antioxidant enzymes, after exposure of tobacco plants to 100 μM AgNPs and AgNO₃, exhibited a decrease or no change in total activity (Cvjetko et al. 2018). It is known that Ag⁺ ions can inhibit enzyme activities by binding to thiols and other active groups or by displacing native metal cations from their binding sites in enzymes (Ghandour et al. 1988). AgNPs applied in this survey were found to be rather stable according to stability analysis. However, 1% dissociation of Ag⁺ was measured in the exposure solution after 7-day period. Moreover, it is possible that detected intracellular AgNPs dissociate into highly toxic Ag⁺ ions, as has been reported by Jiang et al. (2017). Still, in AgNP-treated plants, contrary to AgNO₃, the levels of ROS and parameters of oxidative stress were similar as in control plants (Cvjetko et al. 2018), indicating differences in defense against oxidative stress between AgNP- and AgNO₃-treated plants.

In the category carbohydrate and energy metabolism, majority of the identified proteins were those involved in glycolysis and alcoholic fermentation as well as in mitochondrion-related energy production. This was expected as roots are non-photosynthetic tissue, dependent on glycolysis and oxidative phosphorylation for their energy supplies (Goodwin and Mercer 1983). It has been reported that expression of several proteins involved in the energy production and metabolism, including enolase, aldolase, pyruvate decarboxylase, and alcohol dehydrogenase (ADH), is increased in organisms exposed to metals due to higher energy demands required for detoxification (Kosová et al. 2018). However, in some organisms, opposite results were obtained after exposure to different metals; for example, proteins involved in mitochondrial respiration were up-regulated after Cd-exposure, but inhibited under Mn-induced stress, suggesting that different mechanisms are triggered by exposure to different metals or caused by a dose-dependent response (Luque-Garcia et al. 2011). In rice roots, the ADH abundance was decreased by AgNP treatment (Mirzajani et al. 2014). In tobacco roots exposed to AgNPs or AgNO₃, we found down-regulation of two glycolysis proteins, GAPDH and TPI, as well as of ADH-like UDP-glucose dehydrogenase, protein involved in subsequent fermentative pathway. Down-regulation was also found for MDH and isocitrate dehydrogenase (IDH), proteins involved in tricarboxylic acid (TCA) cycle, which links glycolysis to the mitochondrial electron transport chain. Moreover, abundance of mitochondrial ATP synthase 24-kDa subunit was also lower after exposure of plants to either AgNPs or AgNO₃, which indicates decreased ATP production. Moreover, mitochondrial translation elongation factor Tu was also down-regulated after both treatments, which together, with the decrease in abundance of glutamine synthetase (GS) and glutamate

dehydrogenase (GDH), key enzymes involved in biosynthesis of glutamate and glutamine amino acids, suggests general reduction in protein synthesis. These results imply loss of ability to maintain energy production under silver-imposed stress. Rodríguez-Celma et al. (2010) suggested that low concentrations of metals induce up-regulation of cellular metabolism as adaptive response, while high metal concentrations cause severe cell deregulation. However, it is possible that in roots of tobacco plants, energy metabolism is decreased in response to (nano)silver-induced stress in order to reduce the excess production of ROS and thus prevent induction of oxidative stress, as has been suggested for drought (Vítámvás et al. 2015). Interestingly, one glycolytic enzyme, enolase, was up-regulated under both treatments. Beside its role in glycolysis, enolase activity is required for secondary cell wall assembly and synthesis of lignin, a major structural component of secondary cell walls, which protects cell wall polysaccharides from degradation (Vanholme et al. 2010); therefore,

its enhancement could be involved in defense response against silver stress.

NDPK1, which was found to be down-regulated after treatment with AgNPs and up-regulated after exposure to AgNO₃, is a housekeeping enzyme present in several subcellular compartments, although the main isoform is located in the cytosol (Dorion et al. 2017). NDPK1 plays a specific role in the supply of UTP, necessary for synthesis of cell wall precursors during early root growth (Dorion et al. 2006). Moreover, it was demonstrated that protein moonlighting can be ascribed to NDPK1. Moonlighting proteins perform multiple autonomous and often unrelated functions without partitioning these functions into different domains of the protein (Huberts and Klei 2010). NDPK1 displays important functional diversity by interacting with proteins involved in a variety of processes, including ROS detoxification, carbohydrate metabolism, and signal transduction (Luzarowski et al. 2017). In the study of Dorion et al. (2017), ROS levels were positively correlated

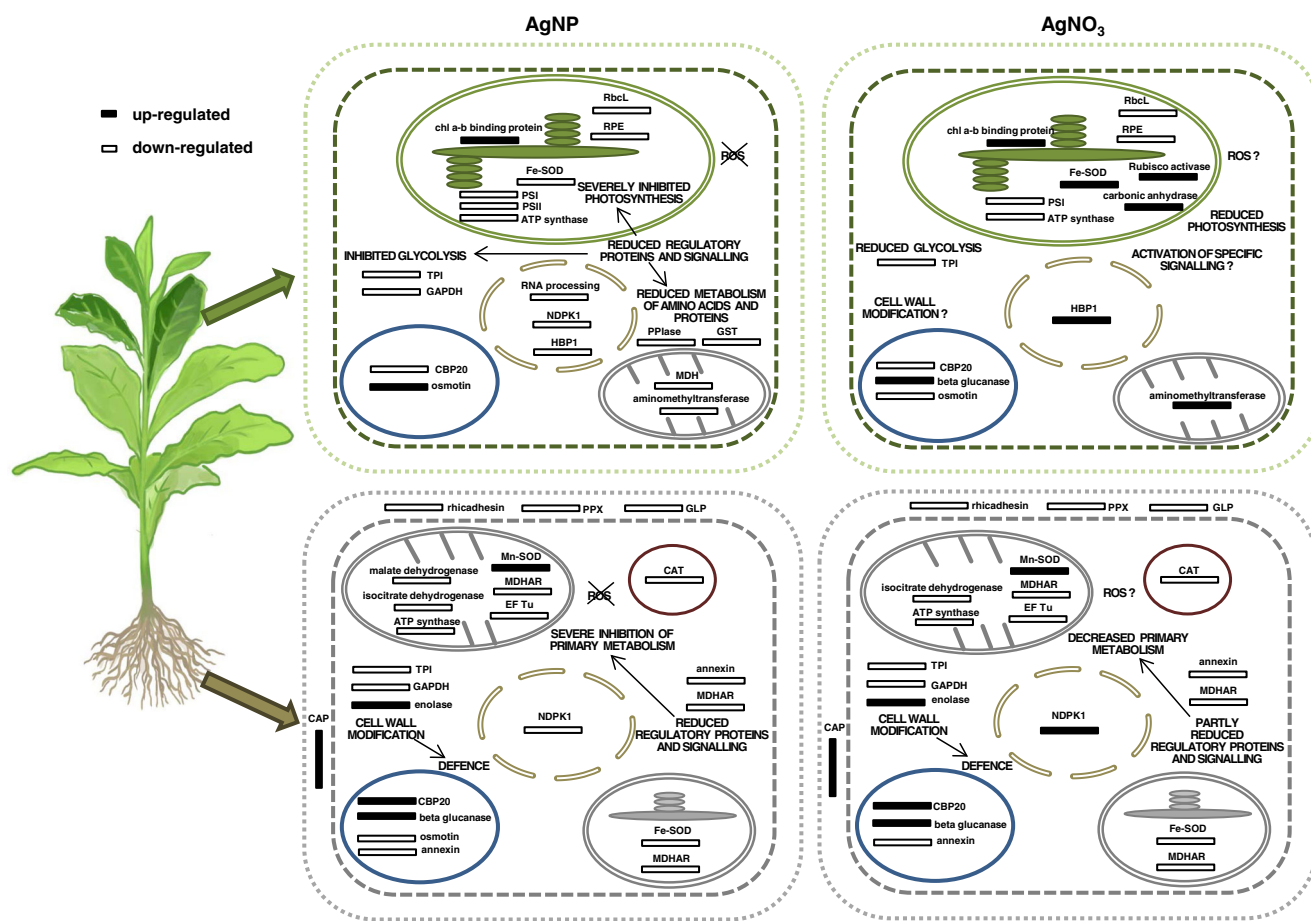


Fig. 7 A schematic comparison of protein abundance in roots and leaves of tobacco adult plant in response to exposure to 100 μM AgNPs or 100 μM AgNO₃. CAP, cysteine-rich secretory protein; CAT, catalase; CBP 20, cap-binding protein 20; EF Tu, elongation factor Tu; Fe-SOD, iron-dependent superoxide dismutase; GAPDH, glyceraldehyde-3-phosphate dehydrogenase; GLP, germin-like protein; GST, glutathione S-transferase; HBP1, ankyrin-repeat protein HBP1; MDH, malate

dehydrogenase; MDHAR, monodehydroascorbate reductase; Mn-SOD, manganese-dependent superoxide dismutase; NDPK1, nucleoside diphosphate kinase 1; PPIase, peptidyl-prolyl cis-trans isomerase; PPX, peroxidase; PSI, photosystem I proteins; PSII, photosystem II proteins; RbcL, Rubisco large subunit; RPE, ribulose-phosphate 3-epimerase; Rubisco activase, ribulose-1,5-bisphosphate carboxylase/oxygenase; TPI, triose phosphate isomerase

with levels of NDPK1 expression in potato roots, which is in agreement with our findings for root tissue; namely, after exposure to AgNO₃, NDPK1 up-regulation as well as increased ROS production (Cvjetko et al. 2018) was recorded, while AgNP treatment resulted in a down-regulation of NDPK1 and control level of ROS (Cvjetko et al. 2018). Moreover, in our previous study, enhanced NDPK1 abundance and increased oxidative stress were found in tobacco seedling exposed to AgNPs and AgNO₃ (Peharec Štefanić et al. 2018).

Leaf proteome

Majority of the identified proteins with differential abundance in leaf tissue were those involved in carbohydrate and energy metabolism. Among biological processes related to this category, photosynthesis was the one on which treatments of tobacco plants with AgNPs and AgNO₃ had the most prominent effect. Among protein complexes engaged in the photosynthesis light-dependent reactions, protein PsaD, which guides ferredoxin (Fd) to the binding site on photosystems I (PSI) (Hanke and Mulo 2013), and protein PsaE, crucial for Fd and ferredoxin-NADP reductase (FNR) binding to PSI (Sétif et al. 2010), were down-regulated after exposure to both treatments. Moreover, FNR, responsible for transferring electrons from Fd to NADP⁺, was also down-regulated after both treatments. In plants exposed to heavy metals like Cd and As, down-regulation of proteins involved in photosynthetic electron transport was also found (Kosová et al. 2018), thus suggesting their susceptibility to metal stress, including (nano)silver, which can result in decreased electron transport and subsequently decreased production of NADPH and ATP. On the other hand, both types of treatments resulted in an up-regulation of chlorophyll *a-b*-binding protein. It is possible that the tobacco plants regulate the abundance of chlorophyll *a-b*-binding protein to preserve the function of PSI and/or photosystems II (PSII) during AgNP- and AgNO₃-induced stress as some proteins from chlorophyll *a-b*-binding family mediate the distribution of excitation energy between PSI and PSII (Andersson et al. 2003). Interestingly, two extrinsic Mn-binding PSII proteins, the 11 kDa one (known as Psb27) and the 23 kDa one (known as PsbP), were down-regulated only after exposure to AgNPs. In *Arabidopsis*, Psb27 homolog is required for the efficient repair of photodamaged PSII (Wei et al. 2010), while the 23-kDa protein plays an important role during the process of PSII assembly (Bondarava et al. 2005). Moreover, CF1 epsilon subunit of plastid ATP synthase, an enzyme involved in ATP biosynthesis, also exhibited decreased abundance in our study after exposure to AgNPs; however, it was up-regulated after the treatment with AgNO₃. Our results are in partial correlation with those of Vannini et al. (2013), who also reported that rocket exposure to AgNO₃ caused up-regulation of plastid ATP synthase subunits, although exposure to AgNPs had no effect on

abundance of this protein. Changes observed in the abundance of the proteins involved in light-dependent reactions can be correlated with previously published chloroplast ultrastructural changes, which differed between AgNP and AgNO₃ treatments, despite similar accumulation of Ag in leaves (Cvjetko et al. 2018). Namely, exposure to 100 μM AgNPs resulted with smaller and partially swollen and ruptured chloroplasts, although the thylakoid system was well developed, while chloroplasts found in leaf cells of AgNO₃-treated plants were bigger than the control ones. These results suggest that exposure to AgNPs and AgNO₃ induces changes in chloroplast ultrastructure and processes that are similar, but not identical, which is evidence that the AgNP effects are not just a result of the release of Ag⁺ ions.

Consistently with decreased primary electron transport processes, photosynthesis carbon reactions were also impaired. Namely, partial Rubisco subunit RbcL of 47 kDa was up-regulated after exposure to either AgNPs or AgNO₃, while the 53-kDa protein, native RbcL, was down-regulated, thus indicating Rubisco degradation. It has already been reported that under metal stress, Rubisco undergoes the down-regulation or degradation (Kosová et al. 2018). It is likely that the reduction in Rubisco content in leaves of tobacco plants exposed to (nano)silver led to a down-regulation of proteins involved in photosynthetic electron transport as an imbalance between the rate of primary and secondary photosynthetic reactions enhances a risk of ROS formation (Kosová et al. 2018). Another enzyme of Calvin cycle, ribulose-phosphate 3-epimerase (RPE), had lower abundance after both treatments, contributing to the diminished photosynthetic activity. However, Rubisco activase 2, enzyme that is required for activation of Rubisco, was up-regulated after exposure to AgNO₃, probably to compensate decreased Rubisco content. Keown et al. (2013) suggested that Rubisco activase removes inhibitors from Rubisco, thus playing a key role in regulating photosynthesis in plants. Moreover, the abundance of beta-carbonic anhydrase, which catalyzes conversion of HCO₃⁻ to CO₂, to ensure the sufficient amount of CO₂ for fixation by Rubisco, was also enhanced after exposure to AgNO₃. Vannini et al. (2013) recorded carbonic anhydrase up-regulation in rocket plants exposed to AgNO₃, which corroborates our results. These results further confirm that AgNPs and AgNO₃ can induce different responses. More severe down-regulation of photosynthesis observed after exposure to AgNPs could be correlated with absence of ROS and oxidative stress in these plants. It can be assumed that by repression of photosynthesis-related proteins, plants avoid damage of the photosynthetic machinery and formation of free radicals that are destructive for the cell (Nouri et al. 2015).

The second group of reactions of the primary metabolism whose proteins were affected with both treatments is glycolysis. In plants, glycolysis takes place in the cytosol and in plastids of both photosynthetic and non-photosynthetic

organs. Down-regulation of glycolysis proteins GAPDH and TPI as well as plastidic aldolase was recorded upon exposure to AgNPs or AgNO₃. MDH, a TCA enzyme, was down-regulated only after exposure to AgNPs. Although an enhanced need for energy under stress conditions often leads to an increase in proteins related to anaerobic metabolism (Kosová et al. 2018), decreased abundance of glycolysis proteins has also been recorded, for example, in cactus tissue exposed to salinity and mannitol (Rogić et al. 2015) and *Arabidopsis* shoots exposed to drought and heat stress (Zeng et al. 2016). It is possible that the negatively affected primary metabolism observed in both tissues might be a consequence of reduced growth due to silver-imposed toxicity.

Besides the inhibition of the primary metabolism, the proteome analysis suggests reduced protein synthesis. Peptidyl-prolyl cis-trans isomerase (PPIase), an enzyme that accelerates protein folding, was found to be down-regulated after exposure to AgNPs. Chloroplastic 30S ribosomal protein S5, an RNA-binding protein responsible for the synthesis of chloroplast genome-encoded proteins, exhibited decreased abundance after both treatments. Since this protein is involved in the synthesis of chloroplast transcription and translation machinery and components of the photosynthetic apparatus (Yamaguchi and Subramanian 2000), its decrease, together with increased abundance of chloroplastic-like protease Do-like 1, protease involved in the degradation of damaged proteins, could explain severe down-regulation of photosynthesis-involved proteins.

Proteins involved in metabolism of amino acids and nucleotides, aminomethyltransferase, glutathione S-transferase (GST), and NDPK1, were down-regulated by AgNPs. This could be a result of reduced primary metabolism and supply shortage. However, aminomethyltransferase, involved in the metabolism of glycine, was up-regulated by AgNO₃, which implies its role in defense response as glycine could be used for synthesis of glycinebetaine, an effective protectant against abiotic stress (Chen and Murata 2008).

In the category defense and stress response, we identified PR protein CBP20, osmotin, and β -1,3-glucanase as well as Fe-SOD, which were also detected in root tissue, although with different abundance level. Lower abundance of CBP20 in leaves after both treatments could be related to much lower silver content accumulated in leaf and, therefore, reduced need for protection against metal-induced damage. However, β -1,3-glucanase exhibited enhanced abundance in leaf after the treatment with AgNO₃, although the content of silver after both treatments was similar. Furthermore, osmotin, a protein that can act as signalling molecule and/or transcriptional regulator (Hakim Ullah et al. 2018) was up-regulated after exposure to AgNPs and down-regulated after exposure to AgNO₃, unlike ankyrin-repeat-containing protein, that regulates expression of PR proteins and antioxidant metabolism (Yan et al. 2002), which was down-regulated after exposure to

AgNPs but up-regulated upon the AgNO₃ treatment. The same response was observed for Fe-SOD and could be related with AgNO₃-induced oxidative stress (Cvjetko et al. 2018). Different abundance of regulatory proteins including two RNA-binding proteins in response to AgNPs or AgNO₃ implies differences in signalling pathway between Ag⁺ ions and nanoparticles, which in turn leads to different expression of other proteins.

Conclusion

The obtained results indicate that in tobacco, AgNPs and AgNO₃ cause similar changes in the root proteome while more distinct changes in the proteome of leaf cells were found. In both tissues, AgNPs revealed more severe impacts on proteome composition in comparison to AgNO₃. Moreover, these data add further evidence that the AgNP effects are not simply due to the release of Ag⁺ ions, but could involve differences in signalling pathway in response to Ag⁺ ions or nanoparticles.

Acknowledgments Tobacco seeds were provided from the Zagreb Tobacco Institute. Authors wish to thank Mr. Juraj Balen for technical assistance in graphical design of figures.

Funding information Performed analyses were supported by the Croatian Science Foundation [grant number IP-2014-09-6488] and the University of Zagreb [grant number 20283115]. TEM analyses have received funding from the European Union Seventh Framework Programme under Grant Agreement 312483 - ESTEEM2 (Integrated Infrastructure Initiative - I3).

Compliance with ethical standards

Conflict of interest The authors declare that they have no conflict of interest.

Abbreviations ADH, alcohol dehydrogenase; AgNPs, silver nanoparticles; ATP, adenosine triphosphate; CBB, Commassie Brilliant Blue; CBP, cap-binding protein; CHAPS, 3-((3-cholamidopropyl) dimethylammonio)-1-propanesulfonate; CHCA, alpha-cyano-4-hydroxycinnamic acid; Cu/Zn-SOD, copper/zinc-dependent superoxide dismutase; DTT, dithiothreitol; EF Tu, elongation factor Tu; EDTA, ethylenediaminetetraacetic acid; EDX, electron dispersive X-ray; Fd, ferredoxin; Fe-SOD, iron-dependent superoxide dismutase; FNR, ferredoxin-NADP reductase; GAPDH, glyceraldehyde-3-phosphate dehydrogenase; GDH, glutamate dehydrogenase; GLP, germin-like protein; GO, gene ontology; GS, glutamine synthetase; GST, glutathione S-transferase; ICP-MS, inductively coupled plasma mass spectrometry; IDH, isocitrate dehydrogenase; IEF, isoelectric focusing; IPG strips, immobilized pH gradient strips; KCl, potassium chloride; LOQ, limit of quantification; MALDI-TOF/TOF, matrix-assisted laser desorption/ionization-time-of-flight/time-of-flight; MDH, malate dehydrogenase; Mn-SOD, manganese-dependent superoxide dismutase; NADP⁺, nicotinamide adenine dinucleotide phosphate; NADPH, reduced form of NADP⁺; NCBIprot, National Center for Biotechnology Information protein database; NDPK1, nucleoside diphosphate kinase; PCA, principal component analysis; PMSF, phenylmethylsulfonyl fluoride; PPIase, peptidyl-prolyl cis-trans isomerase; PR proteins, pathogenesis-related proteins; PSI, photosystem I; PSII, photosystem II; RbcL, Rubisco large subunit; ROS, reactive

oxygen species; RPE, ribulose-phosphate 3-epimerase; Rubisco, ribulose-1,5-bisphosphate carboxylase/oxygenase; SDS-PAGE, sodium dodecyl sulphate-polyacrylamide gel electrophoresis; TCA cycle, tricarboxylic acid cycle; 2-DE, two-dimensional electrophoresis; TEM, transmission electron microscope; TFA, trifluoroacetic acid; TPI, triose phosphate isomerase; UDP, uridine diphosphate; UniProt, Universal Protein Resource; UTP, uridine triphosphate; VCaB42, vacuole-associated annexin protein I

References

- Alvarez S, Berla BM, Sheffield J, Cahoon RE, Jez JM, Hicks LM (2009) Comprehensive analysis of the *Brassica juncea* root proteome in response to cadmium exposure by complementary proteomic approaches. *Proteomics* 9:2419–2431. <https://doi.org/10.1002/pmic.200800478>
- Andersson U, Heddad M, Adamska I (2003) Light stress-induced one-helix protein of the chlorophyll *a/b*-binding family associated with photosystem I. *Plant Physiol* 132:811 LP–811820
- Bondarava N, Beyer P, Krieger-Liszka A (2005) Function of the 23 kDa extrinsic protein of Photosystem II as a manganese binding protein and its role in photoactivation. *Biochim Biophys Acta* 1708:63–70. <https://doi.org/10.1016/j.bbabi.2005.01.005>
- Chen THH, Murata N (2008) Glycinebetaine: an effective protectant against abiotic stress in plants. *Trends Plant Sci* 13:499–505. <https://doi.org/10.1016/j.tplants.2008.06.007>
- Cvjetko P, Milošić A, Domijan A-M, Vinković Vrček I, Tolić S, Peharec Štefanić P, Letofsky-Papst I, Tkalec M, Balen B (2017) Toxicity of silver ions and differently coated silver nanoparticles in *Allium cepa* roots. *Ecotoxicol Environ Saf* 137:18–28. <https://doi.org/10.1016/j.ecoenv.2016.11.009>
- Cvjetko P, Zovko M, Peharec Štefanić P, Biba R, Tkalec M, Domijan A-M, Vinković Vrček I, Letofsky-Papst I, Šikić S, Balen B (2018) Phytotoxic effects of silver nanoparticles in tobacco plants. *Environ Sci Pollut Res* 25:5590–5602. <https://doi.org/10.1007/s11356-017-0928-8>
- Domingos RF, Simon DF, Hauser C, Wilkinson KJ (2011) Bioaccumulation and effects of CdTe/CdS quantum dots on *Chlamydomonas reinhardtii* - nanoparticles or the free ions? *Environ Sci Technol* 45:7664–7669. <https://doi.org/10.1021/es201193s>
- Dorion S, Matton DP, Rivoal J (2006) Characterization of a cytosolic nucleoside diphosphate kinase associated with cell division and growth in potato. *Planta* 224:108–124. <https://doi.org/10.1007/s00425-005-0199-3>
- Dorion S, Clendenning A, Rivoal J (2017) Engineering the expression level of cytosolic nucleoside diphosphate kinase in transgenic *Solanum tuberosum* roots alters growth, respiration and carbon metabolism. *Plant J* 89:914–926. <https://doi.org/10.1111/tpj.13431>
- Dunwell JM, Gibbings JG, Mahmood T, Saqlan Naqvi SM (2008) Germin and germin-like proteins: evolution, structure, and function. *Crit Rev Plant Sci* 27:342–347. <https://doi.org/10.1080/0732680802333938>
- Ghandour W, Hubbard JA, Deistung J, Hughes MN, Poole RK (1988) The uptake of silver ions by *Escherichia coli* K12: toxic effects and interaction with copper ions. *Appl Microbiol Biotechnol* 28:559–565. <https://doi.org/10.1007/BF00250412>
- Goodwin TW, Mercer EI (1983) Introduction to plant biochemistry. Pergamon Press, Oxford
- Hakim Ullah A, Hussain A, Shaban M, Khan AH, Alariqi M, Gul S, Jun Z, Lin S, Li J, Jin S, Munis MFH (2018) Osmotin: a plant defense tool against biotic and abiotic stresses. *Plant Physiol Biochem* 123:149–159. <https://doi.org/10.1016/j.plaphy.2017.12.012>
- Hanke G, Mulo P (2013) Plant type ferredoxins and ferredoxin-dependent metabolism. *Plant Cell Environ* 36:1071–1084. <https://doi.org/10.1111/pce.12046>
- Hensel G, Kunze G, Kunze I (1999) Expression of the tobacco gene CBP20 in response to developmental stage, wounding, salicylic acid and heavy metals. *Plant Sci* 148:165–174. [https://doi.org/10.1016/S0168-9452\(99\)00134-X](https://doi.org/10.1016/S0168-9452(99)00134-X)
- Hossain Z, Komatsu S (2013) Contribution of proteomic studies towards understanding plant heavy metal stress response. *Front Plant Sci* 3:310. <https://doi.org/10.3389/fpls.2012.00310>
- Huberts DHEW, van der Klei IJ (2010) Moonlighting proteins: an intriguing mode of multitasking. *Biochim Biophys Acta* 1803:520–525. <https://doi.org/10.1016/j.bbamcr.2010.01.022>
- Jiang HS, Yin LY, Ren NN, Zhao ST, Li Z, Zhi Y, Shao H, Li W, Gontero B (2017) Silver nanoparticles induced reactive oxygen species via photosynthetic energy transport imbalance in an aquatic plant. *Nanotoxicology* 11:157–167. <https://doi.org/10.1080/17435390.2017.1278802>
- Keown JR, Griffin MDW, Mertens HDT, Pearce FG (2013) Small oligomers of ribulose-bisphosphate carboxylase/oxygenase (Rubisco) activase are required for biological activity. *J Biol Chem* 288:20607–20615. <https://doi.org/10.1074/jbc.M113.466383>
- Kosová K, Vítámvás P, Urban MO, Prášíl IT, Renaut J (2018) Plant abiotic stress proteomics: the major factors determining alterations in cellular proteome. *Front Plant Sci* 9:122. <https://doi.org/10.3389/fpls.2018.00122>
- Kunze I, Kunze G, Bröker M, Manteuffel R, Meins F, Müntz K (1998) Evidence for secretion of vacuolar alpha -mannosidase, class I chitinase, and class I beta-1,3-glucanase in suspension cultures of tobacco cells. *Planta* 205:92–99. <https://doi.org/10.1007/s004250050300>
- Laohavisit A, Davies JM (2011) Annexins. *New Phytol* 189:40–53. <https://doi.org/10.1111/j.1469-8137.2010.03533.x>
- Lee K, Bae DW, Kim SH, Han HJ, Liu X, Park HC, Lim CO, Lee SY, Chung WS (2010) Comparative proteomic analysis of the short-term responses of rice roots and leaves to cadmium. *J Plant Physiol* 167:161–168. <https://doi.org/10.1016/j.jplph.2009.09.006>
- Levard C, Hotze EM, Lowry GV, Brown GEJ (2012) Environmental transformations of silver nanoparticles: impact on stability and toxicity. *Environ Sci Technol* 46:6900–6914. <https://doi.org/10.1021/es2037405>
- Luque-García JL, Cabezas-Sánchez P, Camara C (2011) Proteomics as a tool for examining the toxicity of heavy metals. *TrAC Trends Anal Chem* 30:703–716. <https://doi.org/10.1016/j.trac.2011.01.014>
- Luzarowski M, Kosmacz M, Sokolowska E, Jasinska W, Willmitzer L, Veyel D, Skirycz A (2017) Affinity purification with metabolomic and proteomic analysis unravels diverse roles of nucleoside diphosphate kinases. *J Exp Bot* 68:3487–3499. <https://doi.org/10.1093/jxb/erx183>
- McGillcuddy E, Murray I, Kavanagh S, Morrison L, Fogarty A, Cormican M, Dockery P, Prendergast M, Rowan N, Morris D (2017) Silver nanoparticles in the environment: sources, detection and ecotoxicology. *Sci Total Environ* 575:231–246. <https://doi.org/10.1016/j.scitotenv.2016.10.041>
- Mirzajani F, Askari H, Hamzelou S, Schober Y, Römpf A, Ghassempour A, Spengler B (2014) Proteomics study of silver nanoparticles toxicity on *Oryza sativa* L. *Ecotoxicol Environ Saf* 108:335–339. <https://doi.org/10.1016/j.ecoenv.2014.07.013>
- Mustafa G, Sakata K, Hossain Z, Komatsu S (2015) Proteomic study on the effects of silver nanoparticles on soybean under flooding stress. *J Proteomics* 122:100–118. <https://doi.org/10.1016/j.jprot.2015.03.030>
- Nouri M-Z, Moumeni A, Komatsu S (2015) Abiotic stresses: insight into gene regulation and protein expression in photosynthetic pathways of plants. *Int J Mol Sci* 16:20392–20416. <https://doi.org/10.3390/ijms160920392>

- O'Lexy R, Kasai K, Clark N, Fujiwara T, Sozzani R, Gallagher KL (2018) Exposure to heavy metal stress triggers changes in plasmodesmatal permeability via deposition and breakdown of callose. *J Exp Bot* 69:3715–3728. <https://doi.org/10.1093/jxb/ery171>
- Pavoković D, Križnik B, Krsnik-Rasol M (2012) Evaluation of protein extraction methods for proteomic analysis of non-model recalcitrant plant tissues. *Croat Chem Acta* 85:177–183. <https://doi.org/10.5562/cca1804>
- Peharec Štefanić P, Cvjetko P, Biba R, Domijan A-M, Letofsky-Papst I, Tkalec M, Šikić S, Cindrić M, Balen B (2018) Physiological, ultra-structural and proteomic responses of tobacco seedlings exposed to silver nanoparticles and silver nitrate. *Chemosphere* 209:640–653. <https://doi.org/10.1016/j.chemosphere.2018.06.128>
- Poynton HC, Lazorchak JM, Impellitteri CA, Blalock BJ, Rogers K, Allen HJ, Loguinov A, Heckman JL, Govindasmaw S (2012) Toxicogenomic responses of nanotoxicity in *Daphnia magna* exposed to silver nitrate and coated silver nanoparticles. *Environ Sci Technol* 46:6288–6296. <https://doi.org/10.1021/es3001618>
- Rico CM, Majumdar S, Duarte-Gardea M, Peralta-Videa JR, Gardea-Torresdey JL (2011) Interaction of nanoparticles with edible plants and their possible implications in the food chain. *J Agric Food Chem* 59:3485–3498. <https://doi.org/10.1021/jf104517j>
- Rodríguez-Celma J, Rellán-Alvarez R, Abadía A, Abadía J, López-Millán A-F (2010) Changes induced by two levels of cadmium toxicity in the 2-DE protein profile of tomato roots. *J Proteomics* 73:1694–1706. <https://doi.org/10.1016/j.jprot.2010.05.001>
- Rogić T, Horvatić A, Tkalec M, Cindrić M, Balen B (2015) Proteomic analysis of *Mammillaria gracilis* Pfeiff. in vitro-grown cultures exposed to iso-osmotic NaCl and mannitol. *Plant Cell. Tissue Organ Cult* 122:127–146. <https://doi.org/10.1007/s11240-015-0756-9>
- Seals DF, Randall SK (1997) A vacuole-associated annexin protein, VCaB42, correlates with the expansion of tobacco cells. *Plant Physiol* 115:753–761. <https://doi.org/10.1104/pp.115.2.753>
- Sétif P, Harris N, Lagoutte B, Dotson S, Weinberger SR (2010) Detection of the photosystem I:ferredoxin complex by backscattering interferometry. *J Am Chem Soc* 132:10620–10622. <https://doi.org/10.1021/ja102208u>
- Su Y, Wang Z, Liu F, Li Z, Peng Q, Guo J, Xu L, Que Y (2016) Isolation and characterization of ScGluD2, a new sugarcane beta-1,3-glucanase D family gene induced by *Sporisorium scitamineum*, ABA, H₂O₂, NaCl, and CdCl₂ stresses. *Front Plant Sci* 7:1348. <https://doi.org/10.3389/fpls.2016.01348>
- Sudisha J, Sharathchandra RG, Amruthesh KN, Kumar A, Shetty HS (2012) Pathogenesis related proteins in plant defense response. In: Mérillon J, Ramawat K (eds) Plant defence: biological control. Progress in biological control, vol 12. Springer, Dordrecht. https://doi.org/10.1007/978-94-007-1933-0_17
- Tiwari M, Krishnamurthy S, Shukla D, Kiiskila J, Jain A, Datta R, Sharma N, Sahi SV (2016) Comparative transcriptome and proteome analysis to reveal the biosynthesis of gold nanoparticles in Arabidopsis. *Sci Rep* 6:21733. <https://doi.org/10.1038/srep21733>
- Vanholme R, Demedts B, Morreel K, Ralph J, Boerjan W (2010) Lignin biosynthesis and structure. *Plant Physiol* 153:895–905. <https://doi.org/10.1104/pp.110.155119>
- Vannini C, Domingo G, Onelli E, Prinsi B, Marsoni M, Espen L, Bracale M (2013) Morphological and proteomic responses of *Eruca sativa* exposed to silver nanoparticles or silver nitrate. *PLoS ONE* 8:e68752. <https://doi.org/10.1371/journal.pone.0068752>
- Vannini C, Domingo G, Onelli E, De Mattia F, Bruni I, Marsoni M, Bracale M (2014) Phytotoxic and genotoxic effects of silver nanoparticles exposure on germinating wheat seedlings. *J Plant Physiol* 171:1142–1148. <https://doi.org/10.1016/j.jplph.2014.05.002>
- Vítámvás P, Urban MO, Škodáček Z, Kosová K, Pitelková I, Vítámvás J, Renaut J, Prášil IT (2015) Quantitative analysis of proteome extracted from barley crowns grown under different drought conditions. *Front Plant Sci* 6:479. <https://doi.org/10.3389/fpls.2015.00479>
- Wang T, Chen X, Zhu F, Li H, Li L, Yang Q, Chi X, Yu S, Liang X (2013) Characterization of peanut germin-like proteins, AhGLPs in plant development and defense. *PLoS ONE* 8:e61722. <https://doi.org/10.1371/journal.pone.0061722>
- Wei L, Guo J, Ouyang M, Sun X, Ma J, Chi W, Lu C, Zhang L (2010) LPA19, a Psb27 homolog in *Arabidopsis thaliana*, facilitates D1 protein precursor processing during PSII biogenesis. *J Biol Chem* 285:21391–21398. <https://doi.org/10.1074/jbc.M110.105064>
- Yamaguchi K, Subramanian AR (2000) The plastid ribosomal proteins. Identification of all the proteins in the 50 S subunit of an organelle ribosome (chloroplast). *J Biol Chem* 275:28466–28482. <https://doi.org/10.1074/jbc.M005012200>
- Yan J, Wang J, Zhang H (2002) An ankyrin repeat-containing protein plays a role in both disease resistance and antioxidation metabolism. *Plant J* 29:193–202. <https://doi.org/10.1046/j.0960-7412.2001.01205.x>
- Zeng L, Deng R, Guo Z, Yang S, Deng X (2016) Genome-wide identification and characterization of Glyceraldehyde-3-phosphate dehydrogenase genes family in wheat (*Triticum aestivum*). *BMC Genomics* 17:240. <https://doi.org/10.1186/s12864-016-2527-3>
- Zhang X-F, Liu Z-G, Shen W, Gurunathan S (2016) Silver nanoparticles: synthesis, characterization, properties, applications, and therapeutic approaches. *Int J Mol Sci* 17:1534. <https://doi.org/10.3390/ijms17091534>

Publisher's note Springer Nature remains neutral with regard to jurisdictional claims in published maps and institutional affiliations.